WATER RESOURCES RESEARCH, VOL. 44, W08454, doi:10.1029/2007WR005912, 2008

Bifurcation dynamics and avulsion duration in meandering rivers by one-dimensional and three-dimensional models

M. G. Kleinhans,[1] H. R. A. Jagers,[2] E. Mosselman,[2,3] and C. J. Sloff[2,3]

Received 24 January 2007; revised 7 September 2007; accepted 28 May 2008; published 30 August 2008.

[1] At river bifurcations, water and sediment are divided over two branches. The dynamics of the bifurcation determine the long-term evolution (centuries) of the downstream branches, potentially leading to avulsion, but the dynamics are poorly understood. The long-term evolution can only be studied by one-dimensional models because of computational costs. For such models, a relation describing the sediment division is necessary, but only few relations are available and these remain poorly tested so far. We study the division of sediment and the morphodynamics on a timescale of decades to centuries by idealized three-dimensional modeling of bifurcations with upstream meanders and dominantly bed load transport. An upstream meander favors one bifurcate with more sediment and the other with more water, leading to destabilization. The bifurcations commonly attain a highly asymmetrical division of discharge and sediment after a few decades to a few centuries, depending on combinations of the relevant parameters. Although past work on avulsions focused on slope advantage, we found that bifurcations can be quasibalanced by opposing factors, such as a bifurcate connected to the inner bend with a downstream slope advantage. Nearly balanced bifurcations develop much slower than unbalanced bifurcations, which explains the observed variation in avulsion duration in natural systems. Which branch becomes dominant and the timescale to attain model equilibrium are determined by the length of the downstream bifurcates, the radius of the upstream bend, a possible gradient advantage for one bifurcate and, notably, the width–depth ratio. The latter determines the character of the bars which may result in overdeepening and unstable bars. The distance between the beginning of the upstream bend and the bifurcation determines the location of such bars and pools, which may switch the dominant bifurcate. In fact, when the bifurcation is quasibalanced by opposing factors, any minor disturbance or a different choice of roughness or sediment transport predictor may switch the dominant bifurcate. The division of sediment is nearly the same as the division of flow discharge in most runs until the discharge division becomes very asymmetrical, so that a bifurcate does not close off entirely. This partly explains the sustained existence of residual channels and existence of anastomosing rivers and the potential for reoccupation of old channel courses. We develop a new relation for sediment division at bifurcations in one-dimensional models incorporating the effect of meandering. The flow and sediment divisions predicted by two existing relations and the new relation for one-dimensional models are in qualitative agreement with the three-dimensional model. These one-dimensional relations are however of limited value for wider rivers because they lack the highly three-dimensional bar dynamics that may switch the direction of bifurcation evolution. The potential effects of bed sediment sorting, bank erosion, and levee formation on bifurcation stability and avulsion duration are discussed.

Citation: Kleinhans, M. G., H. R. A. Jagers, E. Mosselman, and C. J. Sloff (2008), Bifurcation dynamics and avulsion duration in meandering rivers by one-dimensional and three-dimensional models, *Water Resour. Res.*, *44*, W08454, doi:10.1029/2007WR005912.

1. Introduction

1.1. Review

[2] Bifurcations distribute water, sediment and, indirectly, flooding risks over the downstream river branches. Over a much longer time, fluvial plains and river deltas are built up by avulsing and (temporarily) bifurcating rivers. For example, the river Rhine in the Netherlands had about

[1]Faculty of Geosciences, Department of Physical Geography, Utrecht University, Utrecht, Netherlands.
[2]Deltares (formerly WL Delft Hydraulics), Delft, Netherlands.
[3]Faculty of Civil Engineering and Geosciences, Delft University of Technology, Delft, Netherlands.

0043-1397/08/2007WR005912$09.00

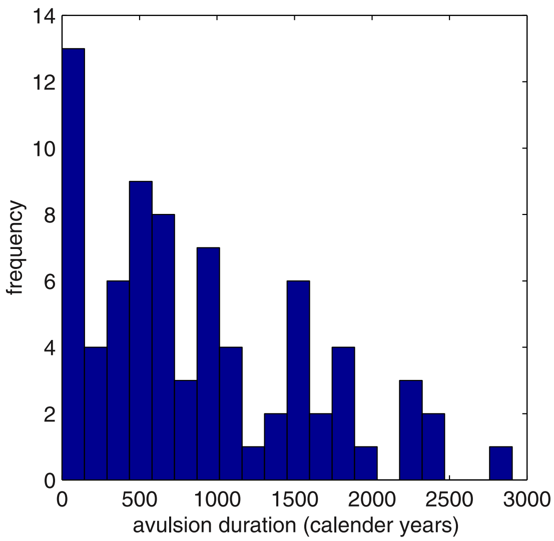

Figure 1. Histogram of avulsion duration in the Rhine derived from the reconstructed avulsions and the ^{14}C datings of the beginning and ending of channel belt activity presented in the works by *Berendsen and Stouthamer* [2000] and *Stouthamer and Berendsen* [2001]. These data exclude about 30 bifurcations that would have ''avulsion'' durations for the entire period of activity of their upstream channels (E. Stouthamer, personal communication, 2005). Note that the ending of channel belt activity itself is governed by bifurcations and avulsion even further upstream.

120 bifurcations in the past 8000 years, some of which were destabilized within a few decades after their creation, whereas other ones were stable for many centuries [*Stouthamer and Berendsen*, 2000, Figure 1]. This striking contrast has not been explained. In addition, bifurcation studies so far concentrated on straight channels while ignoring effects of meander bends just upstream of the bifurcation.

[3] An avulsion site is at least temporarily a bifurcation because the new channel develops while the old one is still active. Also, anabranching or anastomosing rivers by definition have bifurcations, of which long-term pattern stability suggests stable bifurcations. The local morphology of the bifurcation determines its further development, such as a resistant lip in the levee at the entrance of the new channel [*Slingerland and Smith*, 1998], the amount of sediment entering the new bifurcate [*Wang et al.*, 1995; *Bolla Pittaluga et al.*, 2003; *Smith et al.*, 1998; *Slingerland and Smith*, 1998], the angle of the bifurcation on the upstream flow direction [*Bulle*, 1926; *Klaassen et al.*, 1993; *Federici and Paola*, 2003; *Bertoldi et al.*, 2006], migrating bars [*Hirose et al.*, 2003; *Miori et al.*, 2006a] and the presence of an upstream meander favoring one bifurcate with more sediment and the other bifurcate with more discharge [*Kleinhans et al.*, 2006]. Human interference by spur dikes, levees, groynes, meander cutoffs and canals may significantly affect the further evolution, though not always as intended [*van de Ven*, 1976].

[4] In physical process terms, the bifurcation is unstable if one channel receives less sediment than its transport capacity, so that it erodes, and the other channel receives more than its transport capacity, so that it silts up. Hence the division of flow and sediment determines the bifurcation stability or avulsion duration.

[5] The division of flow and sediment is affected by a combination of regional factors, i.e., upstream and downstream boundary conditions, and local factors. *Regional* factors commonly are *external* as they comprise the boundary conditions that are unaffected by the local evolution. The *local* factors commonly are *internal* because they evolve as a result of the internal system dynamics (bar and meander dynamics). Yet the downstream boundary conditions in nature may change due to bifurcation dynamics in rivers with significant backwater effects. For example, a delta connected to one bifurcate may prograde [*Parker et al.*, 2006] or be removed by nearshore processes [*Swenson*, 2005], mouth bars may migrate and levees may prograde [*Edmonds and Slingerland*, 2007], or tidal inlets may evolve [*Stouthamer*, 2005], or the hydraulic resistance or other characteristics of one bifurcate changes, for example due to vegetation development or other changes in the floodplain. This will affect the discharge division of the bifurcation if these downstream developments are within the backwater adaptation length or significantly change the downstream water level by backward migrating erosion or sedimentation [*Kriele et al.*, 1998; *Kleinhans et al.*, 2007a]. In addition, bifurcations that are part of a braided, distributary, anabranching or anastomosing network will be affected by changes in discharge from upstream due to upstream bifurcation or avulsion evolution [*Makaske et al.*, 2002; *Stouthamer*, 2005; *Bertoldi et al.*, 2006]. Hence the temporal and spatial scale of interest depends on the aim of the study, and we will demonstrate that external factors strongly affect the bifurcation evolution. In short, we study an open system that is sensitive to its initial and boundary conditions in addition to internal processes [*Kleinhans et al.*, 2005].

1.2. Objectives and Setup

[6] In order to understand bifurcations and avulsion, the local water and sediment transport division must be understood. Since this is affected by initial and boundary conditions as well as internal processes, combinations are needed of observations, historical maps, historical data and geological reconstructions with models [*Kleinhans et al.*, 2005]. However, two-dimensional and three-dimensional models are computationally too expensive for long-term morphological predictions, and precise historical input data are usually unavailable. A one-dimensional model could then be used, but this has to be extended with a ''nodal point relation'' for dividing the sediment at the bifurcation. Nodal point relations that capture the most relevant processes are difficult to formulate, not in the least because these relevant processes are not entirely understood. An empirical formulation is not feasible as accurate measurements of bed level evolution and sediment transport rates at meandering river bifurcations are rare for single events [*Kleinhans et al.*, 2007b; *Frings and Kleinhans*, 2008] and nonexistent for periods long enough to cover significant changes in morphology and discharge division. We therefore focus on systematic idealized modeling with a three-dimensional model. The definition of the model is

loosely based on the river Rhine in the Netherlands but results are also presented in nondimensional form to facilitate generalization.

[7] The objectives of the work presented here are to understand the causes of bifurcation (in)stability in meandering rivers and the wide range of avulsion durations, and to test and improve nodal point concepts to aid future one-dimensional modeling. In particular, we seek understanding of the effect of (1) meander bends of varying radii and lengths upstream of the bifurcation, (2) bar dynamics upstream of the bifurcation, (3) differences in gradient and length of the downstream bifurcates, (4) floods compared to a sustained representative constant discharge, and (5) combinations of counteracting effects.

[8] In the theory chapter, we first review existing nodal point concepts for one-dimensional models and their assumptions to be tested by the three-dimensional modeling. Since their main shortcoming is that bends upstream of the bifurcation are neglected, we then summarize a simplified version of the theory underlying the three-dimensional model that explains bar dynamics in bends. Based on this, we hypothesize how the bar behavior of the upstream channel may affect the sediment division at bifurcations. Then we propose a new nodal point relation based on the simplified theory. The methods chapter summarizes the setup, numerical aspects, boundary conditions and settings of the one-dimensional and three-dimensional models. The sensitivity to the grid size is first assessed by comparing results with finer and coarser grids. After presenting the main three-dimensional modeling results, extra sensitivity analyses are carried out to assess the effect of an alternative way to schematize bifurcations and of choices of sediment transport and roughness formulations. In the subsequent chapter the three-dimensional model results are compared in detail to one-dimensional nodal point concepts and one-dimensional model runs. After discussing the effects of bars and the applicability of nodal point relations in detail, the general implications for bifurcation stability and avulsion duration are discussed. Furthermore, effects are discussed that were ignored in the modeling, namely bed sediment sorting, bank erosion and floodplain formation. Finally the results are used to explain the sustained existence of residual channels and anastomosing rivers, and conclusions are drawn.

2. Theory and Hypotheses on Sediment Distribution at Bifurcations

[9] We will first review how bifurcations have been incorporated in one-dimensional models, in particular the relations by *Wang et al.* [1995] and by *Bolla Pittaluga et al.* [2003] which predict the sediment division at the bifurcation in response to the flow division. Both relations ignore upstream bars and bends. The theory for bars and bends used in the three-dimensional flow model is simplified to two dimensions. Through analysis of the simplified theory we formulate hypotheses for the effects of upstream channel bends and bars on a bifurcation. Moreover, we will use the simplified theory to formulate a new nodal point relation for one-dimensional models that is consistent with the three-dimensional model. Finally we will list the aspects and assumptions of the two published relations and the new relation that will be tested against the three-dimensional model runs.

2.1. Nodal Point Concepts for One-Dimensional Models

[10] A one-dimensional model of a river with a bifurcation consists of three branches connected by a node. At the node, discharge and sediment supply from the upstream branch (1) is divided over the two downstream branches (the bifurcates 2, 3). The division of flow discharge Q_1 into Q_2, Q_3 at the nodal point follows from mass conservation, the condition that the water levels in the three branches are equal at the nodal point and the characteristics of the bifurcates. The division of sediment cannot be determined from these conditions alone: a nodal point relation is needed to divide the upstream depth–width-integrated sediment transport $Q_{s1} = W_1 q_{s1}$ over the two bifurcates as Q_{s2}, Q_{s3}, where W = width and q_s = specific transport rate. The nodal point relations by *Wang et al.* [1995] and *Bolla Pittaluga et al.* [2003] are briefly reviewed below to describe main aspects and assumptions that will be tested with the three-dimensional model results.

[11] It must be noted here that the model by *Slingerland and Smith* [1998] is in fact also a nodal point relation, but one that refers to the initial stages of avulsion. *Slingerland and Smith* [1998] incorporate only suspended load sediment as the bed load cannot enter the new bifurcate yet because of the entrance lip. Our scope is limited to the evolution of already well-developed bifurcates.

[12] The *Wang et al.* [1995] relation is hypothetical:

$$\frac{Q_{s2}}{Q_{s3}} = \left(\frac{Q_2}{Q_3}\right)^k \left(\frac{W_2}{W_3}\right)^{1-k} \tag{1}$$

where k can be determined empirically. Braided river simulation models, landscape simulation models and delta architecture models often implicitly assume a constant k, usually $k = 1$.

[13] *Wang et al.* [1995] found from a nonlinear stability (phase-plane) analysis that bifurcations are stable for $k > n/3$ and unstable for $k < n/3$, where n = effective power on flow velocity u to calculate the sediment transport as $q_s = mu^n$. For *Engelund and Hansen* [1967] $n = 5$; for all transport equations $n > 3$. Intuitive understanding of their findings is offered as follows. As $u = C(hS)^{1/2}$, with C = Chézy roughness coefficient, S = slope and specific discharge $q = hu$, it follows that the sediment transport capacity in a bifurcate is $q_s \propto q^{n/3}$, whereas equation (1) expresses that the sediment supply at the upstream boundary is $q_s \propto q^k$. Suppose the discharge of one bifurcate decreases. The effect of $k > n/3$ would be a much larger decrease of the sediment input than the decrease of the sediment transport capacity. Consequently, the bed of the closing bifurcate is scoured to some extent, which increases the flow discharge capacity of this channel. So $k > n/3$ stabilizes the bifurcation. On the other hand, $k < n/3$ inevitably leads to closure of one of the bifurcates. The rate of closure depends on the sediment transport rate into the closing bifurcate and its width and the length of the channel fill [*Kleinhans et al.*, 2006].

[14] *Bolla Pittaluga et al.* [2003] presented a nodal point relation that assumes $k = 1$ (division of sediment proportional to flow discharge), but also allows for the deflection

of the bed load vector on a transverse slope, which emerges as one bifurcate silts up whereas the other deepens. Hence an important assumption of this model concept is that the bed levels in the bifurcates extend to the area upstream of the bifurcation, thus creating a transverse bed slope. This assumption is corroborated by some experimental evidence [*Bolla Pittaluga et al.*, 2003]. As a result of the deflection the bifurcation often stabilizes, because the transverse slope decreases the sediment transport into the closing bifurcate. In addition, the modeled bifurcations stabilize for conditions close to incipient motion because they used the *Meyer-Peter and Mueller* [1948] transport predictor which contains a threshold for motion. Upstream meander bend effects are ignored. *Miori et al.* [2006b] added erodible banks by allowing a bifurcate to widen by relaxation to a regime-type equation. Symmetrical bifurcations were always unstable as a result of the erodible banks and developed to a highly asymmetrical discharge division.

[15] The *Bolla Pittaluga et al.* [2003] relation is formulated as follows. The velocity in the main flow direction is calculated from $u = Q_1/(h_1 W_1)$ with h_1 at the end of branch 1, where discharge is assumed to be equally distributed over the cross-section. The transverse flow velocity v is calculated from the flow discharge Q_y that crosses a line dividing the upstream channel of the two bifurcates:

$$Q_y = \frac{1}{2}\left(Q_2 - Q_3 - Q_1 \frac{W_2 - W_3}{W_2 + W_3}\right) \tag{2}$$

so that v can be calculated as:

$$v = \frac{Q_y}{h_1 \alpha_W W_1} \tag{3}$$

where $\alpha_W W_1$ is a defined length immediately upstream of the bifurcation along which the flow and sediment cross the dividing line between the two bifurcates. As such, $\alpha_W W_1$ is the distance upstream of the bifurcation at which the transverse slope should disappear. *Bolla Pittaluga et al.* [2003] experimentally derived that $2 < \alpha_W < 3$, approximately, and found that the results are not sensitive to α_W. At the bifurcation, the sediment Q_{s1} transported at the end of branch 1 is divided over the first cells of the two bifurcates proportional to their widths but corrected for transverse sediment flux. Sediment transport q_{sy} takes place in the transverse direction because the sediment transport vector is deflected on the transverse slope:

$$q_{sy} = \tan\beta_s Q_{s1}/W_1 \tag{4}$$

wherein $\tan\beta_s$ follows from:

$$\beta_\tau = \arctan\frac{v}{u} \tag{5}$$

and

$$\tan\beta_s = \sin\beta_\tau - \frac{r}{\sqrt{\theta}}\frac{\delta z}{\delta y} \tag{6}$$

where $\delta z/\delta y$ = transverse slope and $r = 0.3-1$ is specified. (Note that from equation (14) it can be calculated that $r \approx 1.16$ for typical conditions of the three-dimensional models presented in this paper). The transverse transport rate is subtracted from one bifurcate and added to the other as:

$$Q_{s2} = \frac{W_2}{W_2 + W_3} Q_{s1} + q_{sy}\alpha_W W_1 \tag{7}$$

and from mass conservation $Q_{s3} = Q_{s1} - Q_{s2}$. In the numerical solution by *Bolla Pittaluga et al.* [2003] the transverse slope just upstream of the bifurcation is calculated as:

$$\frac{\Delta z}{\Delta y} = \frac{z_{2,1} - z_{3,1}}{\frac{1}{2}W_1} \tag{8}$$

where $z_{bifurcate,1}$ is the bed level of the first cell of bifurcate i = 2, 3. Together with the distance $\alpha_W W_1$ this represents the assumed extension of the bifurcate bed levels into the upstream channel. This completes the nodal point relation as now the sediment division between the bifurcates can be calculated.

2.2. Flow and Sediment Transport in Meander Bends

[16] In the nodal point relations described above upstream bars and bends are ignored. Before hypotheses for their effects on bifurcations are developed, the theory used in the three-dimensional flow model is simplified below to two dimensions in combination with the equations for sediment transport and a parameterization for secondary flow in bends.

[17] Both the spiral flow and transverse bed gradients found in meandering rivers deflect the sediment transport from the main flow direction, which is relevant for us just upstream of a bifurcation. The bed shear stress τ in the s (main flow) direction can be written as [*Struiksma et al.*, 1985]:

$$\tau_s = \rho g \frac{u\sqrt{u^2 + v^2}}{C^2} \tag{9}$$

where ρ = fluid density, g = gravitational acceleration (9.8 m/s^2), u = flow velocity in s direction, v = flow velocity in n direction. The bed shear stress for the n (transverse) direction can be written as:

$$\tau_n = \tau_s \tan\beta_\tau \tag{10}$$

where the direction β_τ of the bed shear stress vector including the effect of spiral flow is [*Struiksma et al.*, 1985]:

$$\tan\beta_\tau = \frac{v}{u} - \arctan A\frac{h}{R} \tag{11}$$

with spiral flow coefficient A given as:

$$A = \frac{2\varepsilon}{\kappa^2}\left(1 - \frac{\sqrt{g}}{\kappa C}\right) \tag{12}$$

where ε = a calibration coefficient of order O(1) for the spiral flow intensity, κ = 0.4 Von Kármán's constant, h = water depth, R = radius of curvature of the streamlines.

This relation is based on the assumptions of gentle bends (about $R/W > 2$ which is true for all cases presented here) and a logarithmic velocity profile.

[18] Note that the three-dimensional model, contrary to the above 2DH approach, does not assume a logarithmic velocity profile nor gentle bends. Yet in the three-dimensional model the sharpness of bends is somewhat limited by cell size and the requirement of cell orthogonality. We also note that the simplified theory above has been implemented in a quasi-three-dimensional (two-dimensional) version of the Delft three-dimensional system, which is significantly faster than, and gives similar results as the full three-dimensional model for river morphology in general [*Lesser et al.*, 2004] and the present bifurcations in particular [*Kleinhans et al.*, 2006].

[19] On a sloping bed the direction β_s of the sediment transport will deviate from that of the shear stress. For the combination of a transverse slope and spiral flow, *Struiksma et al.* [1985] derived:

$$\tan\beta_s = \frac{\sin\beta_\tau - \frac{1}{f(\theta)}\frac{\delta z}{\delta y}}{\cos\beta_\tau - \frac{1}{f(\theta)}\frac{\delta z}{\delta x}} \tag{13}$$

where $\delta z/\delta y$ = transverse slope and $\delta z/\delta x$ = longitudinal slope. The bed slope effect on sediment transport is calculated with an empirical function for $f(\theta)$ derived from flume experiments by *Talmon et al.* [1995], which has been validated for numerous field cases within the Delft three-dimensional model system [see also *Struiksma et al.*, 1985; *Lesser et al.*, 2004]:

$$f(\theta) = 9\left(\frac{D}{h}\right)^{0.3}\sqrt{\theta} \tag{14}$$

where θ is the nondimensional shear stress (Shields number) defined as

$$\theta = \frac{\tau}{(\rho_s - \rho)gD_{50}} \tag{15}$$

in which ρ_s = density of sediment and ρ = density of water.

2.3. Hypothesized Effect of Bars and Overdeepening on Bifurcation Dynamics

[20] Through analysis of the simplified theory summarized above we will now formulate hypotheses for the effects of upstream channel bends and bars on a bifurcation.

[21] From the previous section it follows that the direction of sediment transport may differ from the direction of depth-averaged flow because of gravitational effects on transverse and longitudinal slopes and because of spiral flow. If a bend is situated just upstream of a bifurcation, the bifurcate connected to the inner bend may therefore receive relatively more sediment and the bifurcate connected to the outer bend may therefore receive relatively more water. Thus a bifurcation may be destabilized or stabilized by an upstream bend. A second hypothesis is that combinations may exist of bend radii at the bifurcation and slope advantages of the bifurcate connected to the inner bend that counteract exactly, so that the bifurcation is nearly balanced and the avulsion duration is much longer than in more unbalanced situations.

[22] A third hypothesis is related to the dynamics of bars at bifurcations, which requires more explanation. The steady bed topography in river bends can be understood as a combination of a transversely sloped bed depending on the local channel curvature and a pattern of steady alternate bars induced by upstream variations (or perturbations) in channel curvature. *Struiksma et al.* [1985] identified four characteristic length scales in the linearized equations for the steady alternate bars, namely the adaptation length of the flow λ_w:

$$\lambda_w = \frac{C^2 h}{2g} \tag{16}$$

the adaptation length of a bed disturbance λ_s:

$$\lambda_s = \frac{1}{\pi^2} h \left(\frac{W}{h}\right)^2 f(\theta) \tag{17}$$

the wavelength of the bar L_p:

$$2\pi\frac{\lambda_w}{L_p} = \frac{1}{2}\sqrt{(n+1)\frac{\lambda_w}{\lambda_s} - \left(\frac{\lambda_w}{\lambda_s}\right)^2 - \left(\frac{n-3}{2}\right)^2} \tag{18}$$

and the damping length L_D.

$$\frac{\lambda_w}{L_D} = \frac{1}{2}\left(\frac{\lambda_w}{\lambda_s} - \frac{n-3}{2}\right) \tag{19}$$

[23] The character of bar dynamics (L_p and L_D) is a function of λ_s/λ_w (sometimes called Interaction Parameter IP), which depends strongly on the width–depth ratio W/h (Figure 2). For narrow and deep channels the bars are overdamped, i.e., the transverse slope in bends adapts within a short distance to the bend radius, approximating the axisymmetrical profile for infinitely long bends (so that $\tan\beta_s$ = 0) that can be derived from equations (11), (12), and (13). This bend profile and the associated spiral flow may affect the transverse slope associated to the bifurcation.

[24] For wider and shallower channels, the bars are underdamped. This leads to overdeepening of the outer-bend pool and associated enhancement of the bar in the inner bend just downstream of the entrance of the bend or other perturbations (such as sudden widening, narrowing, bank irregularities and groynes). If bars are underdamped in a bend just upstream of a bifurcation, then the transverse slope at the bifurcation will depend on the length of the bend upstream of the bifurcation.

[25] For very wide and shallow channels, the bars become unstable and theoretically grow in height downstream of the perturbation. Unlike overdamped and underdamped bars, unstable bars depend not only on perturbations upstream but also on perturbations downstream. The resulting bed topography in this condition ranges from pronounced finite-amplitude alternating bars to braided channel patterns [*Mosselman et al.*, 2006]. Overdeepening and unstable bar behavior may cause the transverse slope at the bifurcation to

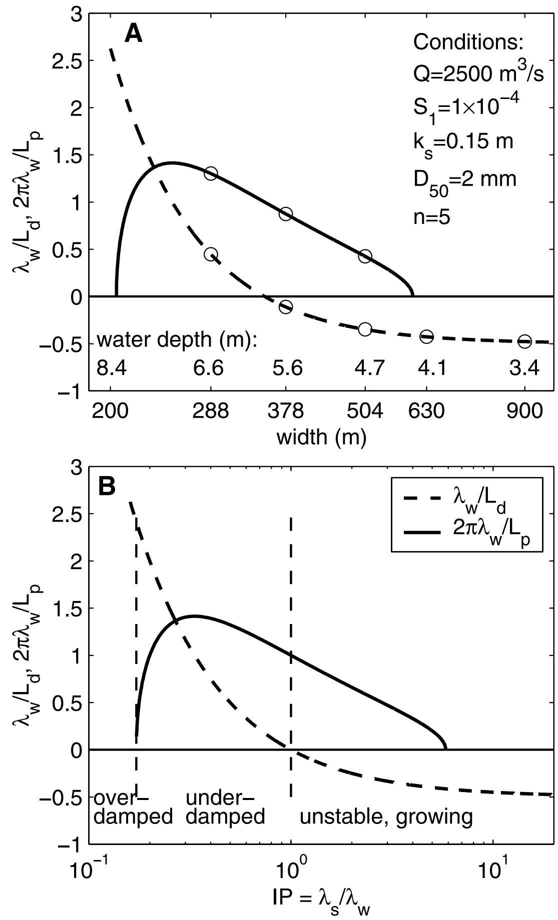

Figure 2. Regimes of bars generated at a perturbation as a function of width (a) and of λ_s/λ_w (b) [after *Struiksma et al.*, 1985]. Overdamped bars (left in b) disappear rapidly, allowing the bend morphology to approximate the axisymmetrical situation over a short length; underdamped bars need more length to damp out and lead to overdeepening in bends, and unstable bars grow in amplitude and initiate more bars downstream. Circles indicate model settings of series 5 in Table 1.

be reversed compared to that in the narrower channels, which would reverse the bifurcation evolution.

[26] The effect of migrating alternating bars on a bifurcation, in contradistinction from the unstable but nonmigrating bars discussed above, may maintain a bifurcation as quasistable with a fluctuating discharge division [*Miori et al.*, 2006a] or a switch bifurcation (main flow switching to the opposite bifurcate [*Hirose et al.*, 2003]).

[27] In short, we hypothesize that the bifurcation dynamics will depend strongly on the width–depth ratio and on the length of the upstream bend (the beginning of which acts as the perturbation that initiates bars). Given that the river Rhine historically had a width–depth ratio on the transition from underdamped to unstable bars [*Schoor et al.*, 1999], this effect will be addressed in the three-dimensional modeling by specifying realistic river widths spanning these two regimes (here 288, 378, 504, 630 and 900 m). The predicted bar wavelength L_p is about 4.0 km for 288 m width, 4.8 km for 378 m, 7.9 km for 504 m and does not exist for 630 and 900 m. However, the bars will be shorter in the beginning as they develop from the initial plane bed, which is relevant for the decisive period of bifurcation evolution. The bars will be damped faster as they migrate into the narrower bifurcates.

2.4. New Nodal Point Relation for Bifurcations With a Bend Upstream

[28] In this section we use the simplified theory to formulate a new nodal point relation for one-dimensional models. Note that the two-dimensional theory has been implemented in the two-dimensional version of Delft three-dimensional, which give nearly the same morphological results for bends and bifurcations [*Lesser et al.*, 2004; *Kleinhans et al.*, 2006]. Thus the nodal point relation developed below is more or less consistent with the three-dimensional model, albeit simplified to one-dimensional.

[29] The *Bolla Pittaluga et al.* [2003] nodal point relation was developed for braided rivers. Compared to meandering rivers, braided rivers have relatively straight, shallow channels where spiral flow can perhaps be neglected. In meandering rivers, which are of interest for the present paper, spiral flow in bends just upstream of bifurcations cannot be neglected. Significantly, extra sediment transport q_{sy} takes place in the transverse direction due to spiral flow, although counteracted by the transverse slope. We will extend the *Bolla Pittaluga et al.* [2003] relation with the deflection by bend flow based on the simplified theory for flow and sediment transport in bends presented earlier. The relations are the same as given in the previous section, except that equation (13) is used for the transverse slope deflection which is combined with the deflection by bend flow by equation (11). For clarity we present the full set of equations again below.

[30] To start, v/u is calculated from $u = Q_1/(h_1 W_1)$ (with h_1 at the end of branch 1) and v from the flow discharge Q_y that crosses the dividing line within a distance of $\alpha_W W_1$ upstream of the two bifurcates as in equation (2):

$$Q_y = \frac{1}{2}\left(Q_2 - Q_3 - Q_1 \frac{W_2 - W_3}{W_2 + W_3}\right) \tag{20}$$

so that v can be calculated as:

$$v = \frac{Q_y}{h_1 \alpha_W W_1} \tag{21}$$

Following *Bolla Pittaluga et al.* [2003], $1 < \alpha_W < 3$. At the bifurcation, the sediment Q_{s1} transported at the end of branch 1 is divided over the first cells of the two bifurcates proportional to their widths. Sediment transport q_{sy} takes place in the transverse direction because the sediment transport vector is deflected on the transverse slope:

$$q_{sy} = \tan \beta_s Q_{s1}/W_1 \tag{22}$$

Herein, $\tan \beta_s$ is not equation (6) combined with equation (5) as in the work of *Bolla Pittaluga et al.* [2003], but the formulations including spiral flow from the work of *Struiksma et al.* [1985] (equation (13) combined with equation (11) and equations (12) and (14)) as follows.

[31] On a sloping bed the direction β_s of the sediment transport deviates from that of the shear stress due to

gravitational effects. For the combination of gravitational effects and spiral flow, [*Struiksma et al.*, 1985] derived equation (13):

$$\tan \beta_s = \frac{\sin \beta_\tau - \frac{1}{f(\theta)} \frac{\delta z}{\delta y}}{\cos \beta_\tau - \frac{1}{f(\theta)} \frac{\delta z}{\delta x}} \tag{23}$$

Herein (equation (11)):

$$\beta_\tau = \arctan \frac{v}{u} - \arctan A \frac{h}{R} \tag{24}$$

wherein the spiral flow coefficient is (equation (12)):

$$A = \frac{2\varepsilon}{\kappa^2} \left(1 - \frac{\sqrt{g}}{\kappa C}\right) \tag{25}$$

with calibration coefficient ε ($\varepsilon = 1$ in the three-dimensional model but will be larger in the one-dimensional model) and under the assumption of gentle bends. The bed slope effect on sediment transport is calculated according to *Talmon et al.* [1995, equation (14)]:

$$f(\theta) = 9 \left(\frac{D}{h}\right)^{0.3} \sqrt{\theta} \tag{26}$$

[32] Having calculated the transverse sediment flux due to a transverse slope and spiral flow, we then continue with the same equations as in the work of *Bolla Pittaluga et al.* [2003]. The transverse transport rate is subtracted from one bifurcate and added to the other as:

$$Q_{s2} = \frac{W_2}{W_2 + W_3} Q_{s1} + q_{sy} \alpha_W W_1 \tag{27}$$

and from mass conservation $Q_{s3} = Q_{s1} - Q_{s2}$. In the numerical solution of the work of *Bolla Pittaluga et al.* [2003] the transverse slope just upstream of the bifurcation is evaluated from the bed levels of the first cells of the bifurcates (2, 3) as:

$$\frac{\Delta z}{\Delta y} = \frac{z_{2,1} - z_{3,1}}{\frac{1}{2} W_1} \tag{28}$$

Together with the distance $\alpha_W W_1$ this forms the extension of the bifurcate bed levels into the upstream channel. This completes the new nodal point relation including the effect of an upstream bend and consistent with a simplified version of the theory underlying the three-dimensional model.

2.5. Tested Aspects and Assumptions of Nodal Point Concepts

[33] The nodal point concepts for one-dimensional models contain a number of aspects and assumptions, which will be tested with the three-dimensional model outcomes:

[34] (1) *Wang et al.* [1995] assume a constant k independent of the stage of development of the closing and opening bifurcate, or both stable bifurcates, and independent of flow conditions such as floods.

[35] (2) *Bolla Pittaluga et al.* [2003] assume that the transverse slope just upstream of the bifurcation extends into the upstream branch over a length of the order of W_1 which remains constant over time. This also implies that the transverse transport Q_{sy} extends over the same distance.

[36] (3) The new nodal point concept presented in section 2.4 assumes that sediment deflection by the spiral flow occurs over the same upstream length as the transverse slope.

[37] (4) The bar regime in the upstream channel is assumed to be overdamped in all nodal point concepts (Figure 2). Upstream bar dynamics will affect the flow direction and the deflection of sediment transport on the transverse slope.

[38] Particularly the last issue has been discussed in the past few years, as *Tubino and Bertoldi* [2005] identified an influence upstream of the bifurcation for the unstable bar regime, in addition to the upstream influence of the downstream boundary condition for water motion. Underdamped bars will affect the transverse slope depending on the length of the bars and the distance between the bifurcation and a perturbation upstream (such as the beginning of the meander bend or a bank irregularity). In addition, the transverse slope will also be affected by perturbations downstream if the bars are unstable.

3. Methodology and Model Description

[39] We will test the nodal point relations and their underlying assumptions in the following steps. Bifurcation evolution as modeled in three-dimensional will be studied in detail for a range of scenarios. Then the flow division calculated in the three-dimensional model will be used to predict the sediment division according to the nodal point relations, and compared to the sediment division calculated in the three-dimensional model. Finally, the nodal point relations will be implemented in a one-dimensional model to compare the morphodynamic evolution to three-dimensional model results.

[40] This chapter is set up as follows. First the one-dimensional and three-dimensional model setup and their boundary conditions are described. Numerical aspects of the three-dimensional model are summarized. Then the scenarios with the three-dimensional model are summarized to provide an overview of all the runs and the sensitivity analyses. Next, alternative model grids are presented for representing bifurcations. Finally, a first sensitivity analysis is performed; we compared model results with grids finer and coarser than used throughout the paper.

3.1. One-Dimensional Model Setup

[41] To test the nodal point relations, a simple one-dimensional research model was set up as follows. The flow in the one-dimensional model is based on the Bélanger equation (backwater formulation, gradually varied flow) with the White–Colebrook roughness predictor. The division of flow discharge Q_1 into Q_2, Q_3 at the nodal point follows from mass conservation and the other specifications: the backwaters up the bifurcates are iterated by varying Q_2, Q_3 until their water levels at the nodal point are equal. The morphology is then updated (first order) by

application of the Exner sediment conservation law with the sediment transport gradient based on the predictor by *Engelund and Hansen* [1967] for all locations except the upstream points of the bifurcates where the nodal point relation is applied.

[42] Each branch has a length of 6 km with a step size of 150 m as in the three-dimensional model. The one-dimensional model is run for 50 years with a (morphological) time step of 0.05 year. The specified model parameters are exactly the same as in the three-dimensional model: upstream discharge ($Q = 2500$ m^3/s), width ($W_1 = 504$ m, $W_2 = W_3 = W_1/2$), Nikuradse roughness length ($k_s = 0.15$ m) and grain size ($D = 2$ mm). The initial bed was plane and had a slope of $S = 1 \times 10^{-4}$ m/m, except where the slope of one downstream channel was deliberately increased as in the three-dimensional model. The downstream water levels were equal to those in the corresponding three-dimensional runs. The upstream sediment transport input was such that the bed level at the upstream boundary did not change during the runs.

3.2. Three-Dimensional Model Setup

[43] The Delft three-dimensional morphodynamic model system was used (version FLOW3.53.01.00, 17 February 2006). The model solves the nonlinear shallow-water equations. *Lesser et al.* [2004] present the full hydrodynamic equations of Delft three-dimensional. These equations are quasi-three-dimensional in the sense that the vertical momentum equation has been reduced to the hydrostatic pressure equation by assuming that vertical flow accelerations are negligible compared with gravity. The three-dimensional model thus consists of several (10 in our case) layers that are coupled through the hydrostatic pressure equation and a continuity equation for mass conservation. This allows an approach in which the horizontal sizes of the computational grid are much larger than the vertical sizes. The flow was calculated according to *Lesser et al.* [2004] on a staggered grid by a second-order ADI scheme based on the dissipative reduced phase error scheme. A third-order upwind ADI transport scheme was used for the standard k–ε turbulence closure model [*Stelling and Leendertse*, 1991]. The time step of the flow was 30 seconds to ensure numerical stability as evaluated by the Courant criterion for fluid advection. An initial period of 50 minutes (or more for longer models) without morphological updating was allowed to stabilize the flow, which was accomplished within the calculation accuracy in about half that time (measured by the convergence of water depth, discharge and velocity to a constant value in time).

[44] Total load transport was computed at cell centers; a first-order upwind Lax scheme was used to determine the bed level changes [*Lesser et al.*, 2004]. Grid cells were converted to dry cells for water depths $h < 0.1$ m. Erosion and sedimentation during a single time step (specified for flow calculation) are very small so that the flow is not affected by morphological change. For more time-efficient calculation, a large number of morphological time steps can be done for each flow time step, expressed as a morphological multiplication factor. The results (bed level change, discharge and sediment division) were not significantly different (i.e., less than 1%) for model runs with factors between 1 and 200. The factor chosen for the model runs presented in this paper was 100.

[45] The imposed boundary conditions are upstream flow discharge, upstream sediment input and downstream water levels. The discharge was constant at $Q = 2500$ m^3/s. Using the flow conditions of the upstream channel and the same transport predictor as in the model, this discharge annually transports an amount of sediment that is equal to the calculated transport using the complete discharge record of the river Rhine of the past century. Initially the discharge is equally divided over the flow width but the distribution is allowed to develop over time as the morphology downstream changes. Given the straight upstream section in all grids this is not significantly affecting the bar pattern evolution in the downstream bend.

[46] The downstream water levels were chosen such that the flow was uniform initially, which results in equal downstream water levels for cases of equal downstream gradients $S_2 = S_3$. The initial bed was plane and had a gradient of $S = 1 \times 10^{-4}$ m/m, except where the gradient of one downstream channel was deliberately increased. The roughness formulation was Darcy–Weissbach with Nikuradse roughness length $k_s = 0.15$ m, and the sensitivity to this choice will be assessed by some runs with a constant Chézy roughness factor C instead.

[47] The sediment transport at the upstream boundary is calculated at transport capacity, preventing bed level change at the boundary. The sediment transport predictor, unless mentioned otherwise, is *Engelund and Hansen* [1967] and the sensitivity to this choice will be assessed later by comparing with runs where *Van Rijn* [1984a, 1984b] was used. The sediment is uniform with size $D_{50} = 2$ mm (used in the work of *Engelund and Hansen* [1967]) and $D_{90} = 8$ mm (only used in the work of *Van Rijn* [1984a] for grain-related shear stress), resulting in dominant bed load transport. The effect of finer sediment ($D_{50} = 0.5$ mm, $D_{90} = 1.5$ mm) with dominant suspended load transport will be assessed later.

3.3. Bifurcation Schematization and Grid Creation

[48] The grids of the three-dimensional model were curvilinear (Figure 3). The grids were generated automatically as concatenated straight and curved sections to ensure repeatability. The grids were orthogonalized as much as possible in an automated procedure minimizing deviations from orthogonality of adjacent cell midpoints by iterative adaptation of cell shape and position while minimizing gradients in cell size and width–length ratio. The average length of the grid cells was 150 m. The width of the cells was 28 m (so that the channel width becomes $W_1 = 504$ m) for the standard models, 35 m ($W_1 = 630$ m) and 50 m ($W_1 = 900$ m) for the wider, and 21 m ($W_1 = 378$ m) and 16 m ($W_1 = 288$ m) for narrower models. The flow was divided vertically into 10 layers of equal thickness (0.47 m initially for 4.7 m water depth), which was automatically adapted to water depth changes during a model run [*Lesser et al.*, 2004]. All three branches had the same lengths and consisted of 40 cells each (6 km), resulting in a grid of 80 cells long, 18 wide and 10 thick. Grids were generated with varying upstream bend radii, whereby short bends were 17 cells long and long bends were 35 cells long; both downstream of a straight stretch (Figure 3). Downstream of the bifurcation a constant bend radius of $R/W_1 = 20$ was specified. Several runs with a bend with a single straight downstream channel are presented to compare how the bed

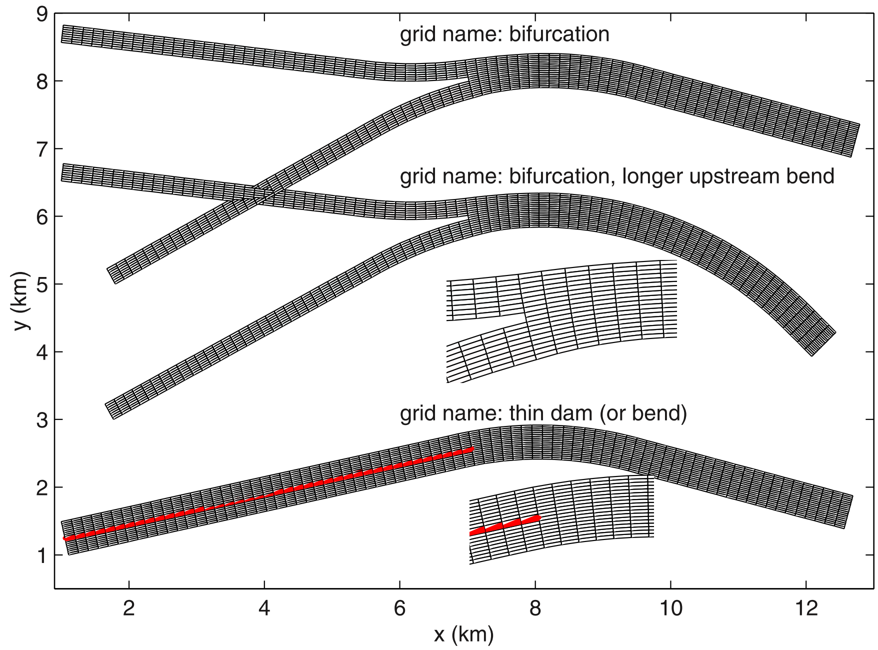

Figure 3. Example grids of a short bend (top; series 1, 2 in Table 1), long bend (middle; series 6), and schematized as a bend with a thin impervious dam (bottom; series 8); all with $R/W_1 = 10$ and $W = 504$ m. The flow is from right to left. Insets shows details at the bifurcation. The upstream channel has index 1, the bifurcate connected to the upstream outer bend (top) has index 2, and that connected to the inner bend (bottom) has index 3 in this paper.

upstream of the bifurcation would have evolved in the absence of the bifurcation.

[49] To split one channel into two at a bifurcation in a curvilinear grid, two rows of cells had to disappear downstream of the bifurcation for numerical reasons (see inset in Figure 3). To ensure that $W_2 + W_3 = W_1$, the width of the cells downstream of the bifurcation was increased (see *Kleinhans et al.* [2006] for two-dimensional runs with $W_2 + W_3 \geq W_1$). The transition to this increased width was done gradually in the five cells upstream of the bifurcation. This choice is based on observations in natural bifurcations and on a rule of thumb that the upstream distance of influence of a disturbance, in this case the bifurcation, is of the order of the channel width.

[50] Some results of an alternative way to schematize a bifurcation are presented: by specifying an infinitely thin, impervious dam (hereafter "thin dam") along the centerline of the downstream half of the aforementioned bends (Figure 3). The thin dam disconnects the cells on its sides and thus divides the downstream half of the grid into two entirely independent (but parallel) bifurcates. As the dam is infinitely thin, it was not necessary to correct the cell width in the bifurcates and the channel width just upstream of the bifurcation was the same as further upstream since no cells had to disappear contrary to the bifurcated grid. Hence any difference in model result between the bifurcated grid and the thin dam grid are due to the (absence of a) bifurcation "bluff" or the grid cell widening.

[51] To demonstrate the negligible grid dependence of the general results, several cases with halved grid cell sizes (horizontal) are presented ($160 \times 40 \times 10$ cells) as well as cases with doubled grid cell sizes. Coarse grids were created by doubling the grid cells in size in the horizontal directions. The bluff at the bifurcation is still 2 cells wide as in the standard grids, but its width is necessarily larger because grid halving was not exactly possible for the bifurcated grid. Thus differing results between coarse and standard grids can be ascribed either to the coarseness of the grid or the different bluff. Fine grids were created by halving the grid cells in the horizontal directions. The bluff at the bifurcation became 4 cells wide with the same total width as in the grids of standard resolution used in the rest of this paper. In addition, one alternative fine grid was created in which the bluff was only two cells wide (as in the standard grid) so that the bluff was two times narrower than in the standard grid. This alternative run was done with equal slopes in the bifurcates.

3.4. Model Scenarios and Generality of the Results

[52] The model settings presented in this paper were loosely based on the river Rhine but designed such that a large range of conditions occurring in natural rivers is covered. Table 1 summarizes the runs.

[53] The first series was to assess the effect of varying bend radius upstream of the bifurcation. As gradient advantage is often cited as a cause of successful avulsion, the second series was to increase the gradient in the bifurcate connected to the inner bend. These runs were all done with relatively short bifurcates while backwater effects are known to be important and the length of the bifurcate may determine the timescale of closure. Therefore a third series was done with bifurcates as long as those in the Rhine delta, which are much longer than the backwater adaptation length. Assessing the importance of floods is computationally expensive because the morphological multiplication factor can no longer be used. Floods are therefore applied for a limited duration only and for cases where the bifurcates are nearly symmetrical as well as for cases where one

Table 1. Overview of Model Runs Presented in This Paper

Series	N	Figure Number	R/W_1	Grid Type	Description
1	8	7[a]	2, 4, 6, 8, 10, 20, 50, 100	bifurcating	varying upstream bend radius, 6 km long branches, 50 years duration
2	6	8	4, 10, 100	bifurcating	increased gradient of inner-bend branch: $S_3 = 1.1S_2$
3	4	9	4, 10	bifurcating	downstream branch length 31 km and 106 km, 200 years duration
4	4	9, 10	4	bifurcating	downstream branch length 106 km, discharge varied
5	4	11, 12 left	10	bifurcating	varying widths: W_1 = 288, 378, 504 (from series 1), 630, 900 m
6	5	11, 12 right	10	bifurcating	longer upstream bend than series 1–5; widths as series 5
7	4	11, 13 left	10	bend	no bifurcation, W_1 = 288, 504 m, short and long bend
8	4	11, 13 right	10	thin dam	bifurcation schematized as bend (as series 7) with thin impervious dam to split bifurcates
9	3	14a, 14b	4, 10, 100	bifurcating	constant Chézy roughness instead of constant Nikuradse k_s
10	8	14g, 14h	2, 4, 6, 8, 10, 20, 50, 100	bifurcating	finer sediment: D_{50} = 0.5 mm instead of D_{50} = 2.0 mm
11	2	14c, 14d	10, 100	bifurcating	*Van Rijn* [1984a, 1984b] sediment transport predictors instead of *Engelund and Hansen* [1967]
12	8	14e, 14f	2, 4, 6, 8, 10, 20, 50, 100	bifurcating	finer sediment: D_{50} = 0.5 mm and *Van Rijn* [1984a, 1984b] transport predictors
13	4	4e, 4f	4, 10, 100	bifurcating	halved grid cells (fine grid), 3 runs with $S_3 = 1.1S_2$; one run with narrow bluff and $S_3 = S_2$ for R/W_1 = 4, 100 years duration
14	3	4a, 4b	4, 10, 100	bifurcating	doubled grid cells (coarse grid), $S_3 = 1.1S_2$; 100 years duration

[a]For R/W_1 = 10: 3, 6, 11a, 15a–15e, 16; for R/W_1 = 4: 15f–15j, for R/W_1 = 4, 10, 100: 4c, 4d. The series label is used as reference in this paper. N is the number of runs in the series. Figure number refers to the figures where these series are presented and grid type is explained in section 3.5. See *Kleinhans et al.* [2006] for more model runs in two-dimensional mode.

bifurcate already nearly closed off (series 4) as it may be conceived that nearly closed bifurcates are much more affected by floods. In the fifth series the width–depth ratio was varied and in the sixth series the length of the upstream bend was increased as both determine bar dynamics at the bifurcation and therefore potentially affect the long-term evolution of a bifurcation.

[54] Series 7–14 in Table 1 are intended for comparison and as sensitivity analyses. To ascertain the effect of the presence of a bifurcation on the upstream bend, runs were done without bifurcations and with exactly the same bends, as well as runs with an alternative representation of bifurcation in a grid (series 7 and 8). Several choices of friction formulation, sediment transport predictors and sediment sizes made in the initial model setup were based on measurements in the river Rhine, on modeling experience and understanding of theory. The sensitivity of the results to these choices was assessed in series 9–12. Finally, the sensitivity of the results to the grid resolution was assessed by comparison of model results to finer and coarser grids (series 13, 14). The grid resolution results will already be presented in the next section to ascertain the validity of our main results.

[55] To put our results in a general perspective, we compare a number of basic nondimensional parameters of the model settings and real terrestrial rivers (Table 2). The nondimensional numbers refer to the specified grids and to the flow and sediment dynamics (of initial stages). The numbers are compared with parameters calculated for the river data set by *Van den Berg* [1995] and empirical relations provided by *Bridge* [2003] and *Camporeale et al.* [2005]. The comparison demonstrates that our results are well within natural ranges of parameters for large meandering and nearly braided rivers, although natural braided

Table 2. Nondimensional Numbers Representing the Model Runs in Comparison to Real-World Values Reported in or Derived From Literature[a]

Description	Parameter	Model	Series	Real World References
Relative bifurcate length	$L_{2,3}/\lambda_{BW}$	0.25–4	1, 3	Rhine bifurcates [*Stouthamer and Berendsen*, 2001] have lengths of 10–200 km for similar flow conditions; lake deltas [*Edmonds and Slingerland*, 2007] have very short, evolving bifurcates
Width–depth ratio	W_1/h_1	44–163	5	data in *Van den Berg* [1995]: W_1/h_1 = 110 ± a factor of 2 for meandering and (wider) braided rivers
Relative bend radius (width)	R/W_1	2–100	1	relations in *Bridge* [2003, Table 5.6]: R/W_1 = 3–14, so our models include nearly straight and rather sharp-bended meandering rivers
Relative bend radius (depth)	$h_1C^2/(8gR)$	$< 7 \times 10^{-3}$	1	relations in *Camporeale et al.* [2005, Figure 5 and 6]: $h_1C^2/(8gR) \approx 4 \times 10^{-2}$, so our models refer to gentle bends in shallow rivers
Froude number	Fr	0.14–0.17	all	data in *Van den Berg* [1995]: $0.1 < Fr < 0.5$ for sand-bed rivers; $0.1 < Fr < 0.9$ for gravel bed rivers
Shields number	θ	0.12–0.8	5, 10	data in *Van den Berg* [1995]: $0.26 < \theta < 0.99$ with decreasing θ for increasing D_{50}
Interaction parameter	IP = λ_s/λ_w	0.5–10	5	data in *Van den Berg* [1995]: $0.1 < \mathrm{IP} < 10$ for $10 < W_1/h_1 < 100$ with a factor 10 spread

[a]The column Model refers to the values imposed on or derived from the three-dimensional modeling; Series refers to the model series in Table 1.

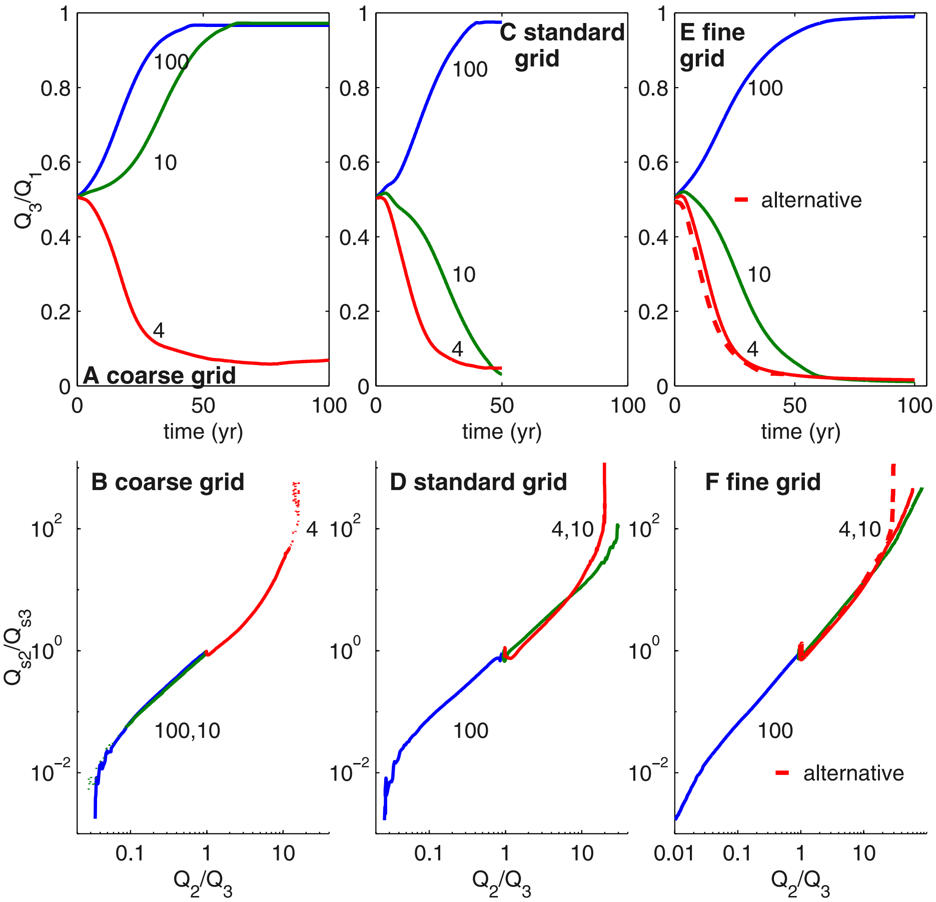

Figure 4. Comparison of discharge and sediment division in the coarse (series 15 in Table 1), standard (as in the rest of this paper, series 2), and fine grids (series 14). (a, c, e) Time series of discharge for the inner-bend bifurcate. Labels indicate R/W_1: bend radius R as a multiple of the upstream channel width W_1. (b, d, f) Sediment and discharge division over the bifurcates. The dashed line in (e) and (f) represents the alternative fine grid with a smaller bluff of only two cells wide and $S_2 = S_3$. The dotted parts of the lines in (b) and (f) represent the 50–100 year time span, during which the closure process in the coarse and fine grids is demonstrated to be similar to the standard grid.

rivers are even wider and shallower. However, our focus was on meandering rivers. The bend radii modeled here are not the sharpest found in nature, for which the model cannot be applied with the present grid, but do include sharp to gentle (nearly straight) river reaches.

3.5. Sensitivity to Grid Size

[56] In this section we present several tests to ascertain the sensitivity of our results to the chosen grid size (series 1, 2, 13, 14 in Table 1). These tests were all done with the "standard" 12 km long grids with short bifurcates and short upstream bends of R/W_1 = 4, 10, 100 and with a 10% steeper slope of the inner-bend bifurcate (except for one fine grid with a narrower bluff), so that the bend and slope advantage effect compete (this will be explained in detail in the results chapter). The model results are the most sensitive to the small net effect near the critical combination of bend radius and inner-bend slope where the bend and slope advantages (nearly) cancel out. In such settings the model results are also sensitive to grid effects which we will employ here to assess the effect of grid size.

[57] The fine grid runs have similar behavior as the standard grid (compare Figure 4e and 4f with Figures 4c and 4d, and Figure 5). In particular, the direction of evolution of the bifurcations is the same: for the bends with R/W_1 = 4, 10 the bend effect overcomes the slope advantage of the inner-bend bifurcate while for the gentler bend the slope effect is dominant. In detail, there are differences: the gentle-bend run in the standard grid stabilizes the discharge division sooner than in the fine grid run. The discharge change in the first 25 years is within a few percent for standard and fine grids but particularly in the closing phase the fine grid models keep their closing bifurcate open for a much longer time while the final discharge asymmetry is more pronounced. The sediment division (Figures 4d and 4e) is also within a few percent until the discharge ratio of the bifurcates is more than 10. Below that ratio, the Q_{s2}/Q_{s3} plotted versus Q_2/Q_3 (Figures 4b, 4d, and 4f) is a straight line in double logarithmic space, which means a constant power k in equation (1). This means that the final near-closure process in the finer grid differs from the coarser grid (discussed later).

[58] The final equilibrium discharge division of the alternative fine grid with the narrow bluff is more asymmetrical than the one of the normal grid (Figure 4), which is due to the finer bed level structure of the closing bifurcate, where

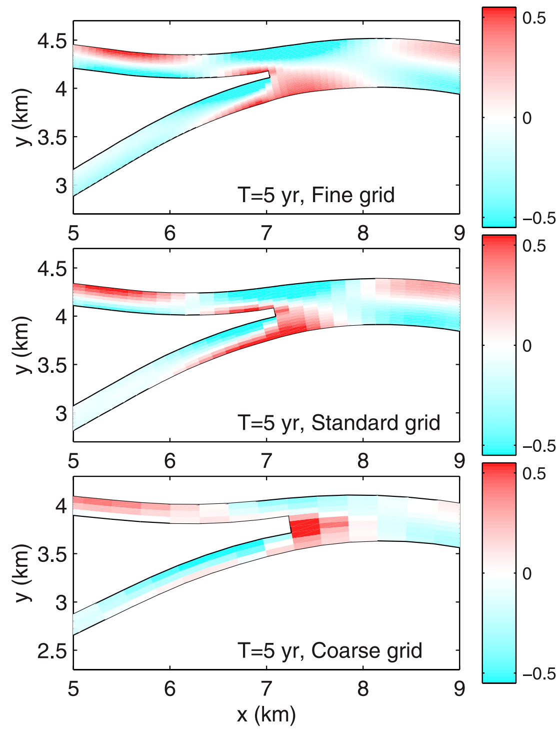

Figure 5. Sedimentation–erosion pattern (scale in meter) of the three-dimensional model at $T = 5$ years with coarse, standard, and fine grid ($R/W_1 = 10$ from series 15, 2, and 14 in Table 1).

some cells become dry while others remain active. This suggests that the bifurcates with even smaller bend radii would have had more (instead of less) asymmetrical equilibrium discharge divisions with finer grids. The morphology is also very similar but slightly more pronounced (plotted as dashed lines in Figure 15). The discrepancy of Q_3/Q_1 between fine and standard grid is at most 10% (for $t = 30$ year and $R/W_1 = 100$), or, the time discrepancy at which the same discharge is attained is 10 years (for $t = 30–40$ year, $R/W_1 = 100$ and $Q_3/Q_1 = 0.9$).

[59] The general behavior of the coarse grids is similar to that of the standard grids (compare Figures 4a and 4b to Figures 4c and 4d). A major difference is that the bifurcation with $R/W_1 = 10$ has flipped: the slope effect dominates over the bend effect in the coarse grid whereas the bend effect dominates in the standard and fine grid. In addition, the sediment division in the coarse grid is different (an increasing power k) after a shorter period and when the bifurcate discharge ratio is above 5 (compared with 10 for fine grid runs). The reason for the deviating behavior of the coarse grid is the initial formation of an extended scour hole just downstream of the bifurcation in the inner-bend bifurcate. This scour hole was also observed in the standard grid and particularly with other sediment transport predictors, but there its deepening was reversed due to the infilling of the inner-bend bifurcate. As said before, this difference may well be due to the wider bluff in the coarse grid rather than the coarser grid itself. In the coarse grid the scour became a few cells long, as in the standard grid, so it was much more extended spatially because the grid cell size was twice as large.

[60] In general, the same conclusions can be drawn from the coarse, standard and fine grids: at certain combinations of upstream bend radius and downstream slope advantage of the inner-bend bifurcate, these two effects cancel out so that the bifurcation remains quasistable. Near the critical combinations the model runs are extremely sensitive to initial and boundary conditions and the grid cell size. These grid size dependence tests therefore demonstrate that the chosen standard grid size is adequate for the modeling of general bifurcation behavior. The most important parameters, namely flow and sediment division, converged for the chosen grid size compared with finer grids, although this does not imply that other modeled parameters have converged as discussed by *Hardy et al.* [2003]. The precise model results are sensitive to the grid resolution, mostly because of the formation of local scour near the bifurcation and because the representation of bar and bend morphology is better on finer grids. For fine grids, the power k remains constant for higher ratios of upstream/downstream discharge than in coarser grids, which means that the final closure process differs for fine grids.

4. Results

[61] In this chapter we present the model results that are most relevant for understanding real bifurcations. These are the effect on bifurcation evolution of an upstream bend in competition with the effect of a downstream slope advantage of the bifurcate connected to the inner bend. Furthermore, the effect of the length of the bifurcates is studied relative to the backwater adaptation length. Next some results are presented on the effect of floods on the long-term morphodynamics. Finally the effects of upstream channel width–depth ratio and the length of the upstream bend are presented because these factors determine bar dynamics which may affect bifurcation evolution.

4.1. Morphodynamics at the Bifurcation and Effect of Bend Radius

[62] The general morphological development in the three-dimensional model with a width of $W_1 = 504$ m and an upstream bend radius of $R/W_1 = 10$ is shallowing of the bifurcate connected to the inner bend and deepening of the outer-bend bifurcate (Figure 6 and series 1 in Table 1). In the first few model years alternating bars develop from the plane bed and migrate downstream. After some time, a fixed bar develops in the inner bend upstream of the bifurcation. Meanwhile, a bar and pool migrate side-by-side into the bifurcates and become fixed in position as well. The rate of bar development and migration depend on the bend radius: the sharpest bends have the fastest development of a fixed bar. The morphological evolution of similar bends without bifurcations will be compared later.

[63] For all bend radii (series 1 in Table 1), the model always predicts a development to a stable, highly asymmetrical discharge division. The outer-bend bifurcate becomes dominant when the downstream conditions in the two bifurcates are equal (Figure 7a). The division of sediment transport is fairly similar to that of the flow (Figure 7b). Initially the flow and sediment division fluctuates in a damped, quasiperiodic manner (phase 1). This is caused by the development and migration of the bars from an initially plane bed. This is seen as the kinks in Figure 7b in the first 10 years and the fluctuations in the lower-left corner of

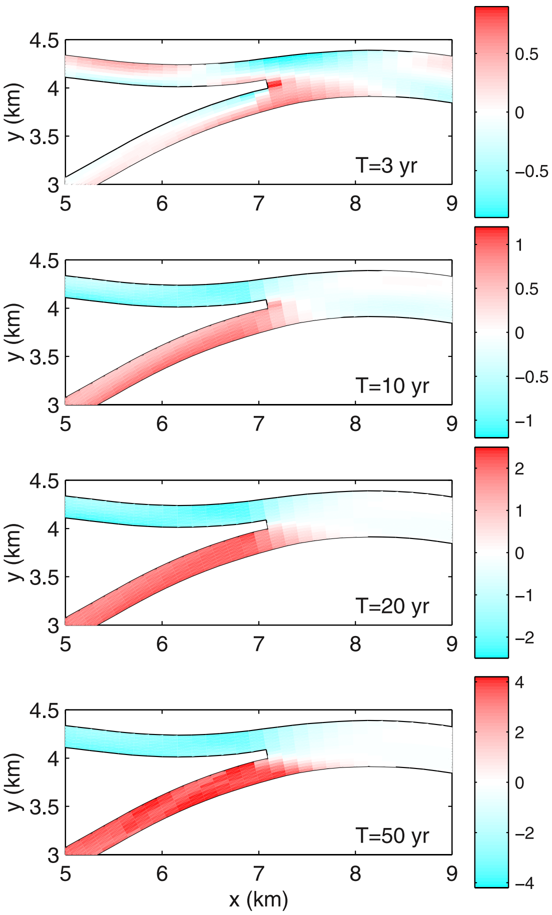

Figure 6. Sedimentation–erosion pattern (scale in meter) of the three-dimensional model with $R/W_1 = 10$ (series 1 in Table 1). At $T = 20$ years, the bed elevation difference between the bifurcates is so large that the upstream bend profile is no longer visible on this color scale.

Figure 7b. Later (phase 2) the flow and sediment are increasingly discharged into one bifurcate and the bifurcates silt up or scour along their whole length, but mostly in their upstream parts. This is seen in Figure 7a as the declining Q_3/Q_1 ratio and in Figure 7b as the straight lines between $1 < Q_2/Q_3 < 10$. Because of the proximity of the fixed downstream water level, the smaller discharge leads to a downstream increasing flow depth associated with flow deceleration which further enhances the aggradation of this bifurcate.

[64] Notably, in the final stages (phase 3) ($Q_2/Q_3 > 10$) the sediment transport declines more rapidly than the discharge, thereby apparently increasing k from a value below to a value above the stability threshold $k = n/3$ where $n = 5$ for the *Engelund and Hansen* [1967] transport predictor. This is caused by two factors. The first factor is the increasing transverse slope of the bed into the closing bifurcate, which deflects the sediment transport into the larger bifurcate. The second factor is the increasing relative roughness k_s/h as $k_s = 0.15$ (constant) while the water depth h decreases. This affects the transport rate, which is proportional to $C^2h^{5/2}$ [*Engelund and Hansen*, 1967], whereas the discharge is proportional to $C\ h^{1/2}$. The discharge in the closing bifurcate then stabilizes at a small but nonzero value.

[65] The model-derived k is slightly larger for sharper bends (also see later graphs), particularly for $R < 5W$ for which the final discharge division is slightly less asymmetrical than for gentler bends. Apparently the bend effect on the flow and sediment division is so large that k is larger in sharper bends than in gentle bends initially. This difference is perhaps affected by the emergence of a scour hole in the inner-bend bifurcate just downstream of the bifurcation, which attracts flow and thus keeps the bifurcate more open.

4.2. Effects of a Downstream Gradient Advantage

[66] Avulsions commonly take place because of a gradient advantage of the new flow direction over the old channel. To test the effect of an increased gradient in one bifurcate, this gradient increase was specified in the initial bed levels and the downstream water levels were adjusted to ensure initial uniform flow. For these runs $W_1 = 504$ m and the bend radii $R/W_1 = 4$, 10, 100 (series 2 in Table 1).

[67] The effect of the upstream bend can be counteracted by increasing the gradient of the inner-bend bifurcate (Figure 8a). Thus this parameter combination determines the direction of bifurcation evolution; that is, the choice which bifurcate becomes dominant. For a gradient increase of 30% (not reported) the inner-bend bifurcate always dominates. For a gradient increase of only 10% ($S_3 = 1.1 \times 10^{-4}$

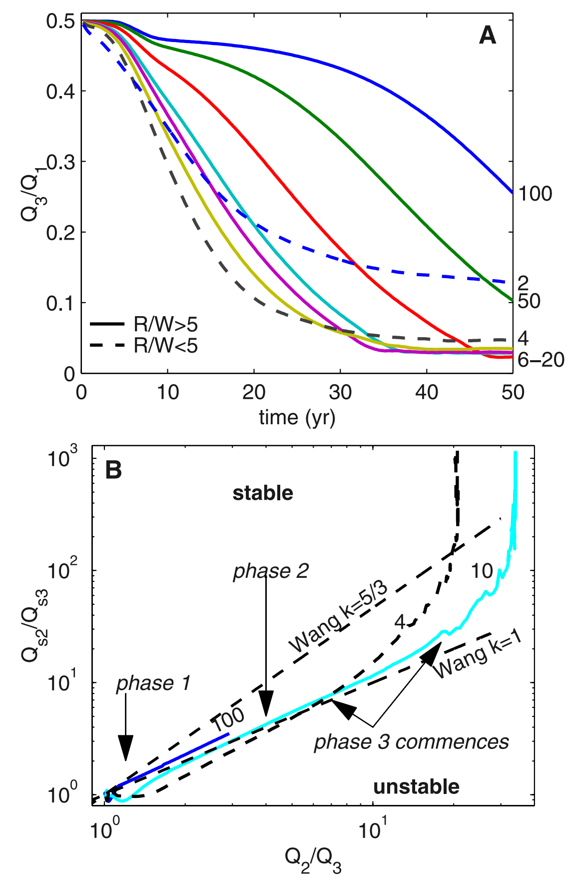

Figure 7. Effect of bend radius on bifurcation evolution according to three-dimensional model (series 1 in Table 1). (a) Time series of discharge for the inner-bend bifurcate. Labels indicate R/W_1: bend radius R as a multiple of the upstream channel width W_1. (b) Sediment and discharge division over the bifurcates compared with the *Wang et al.* [1995] model. For explanation of phases, see text.

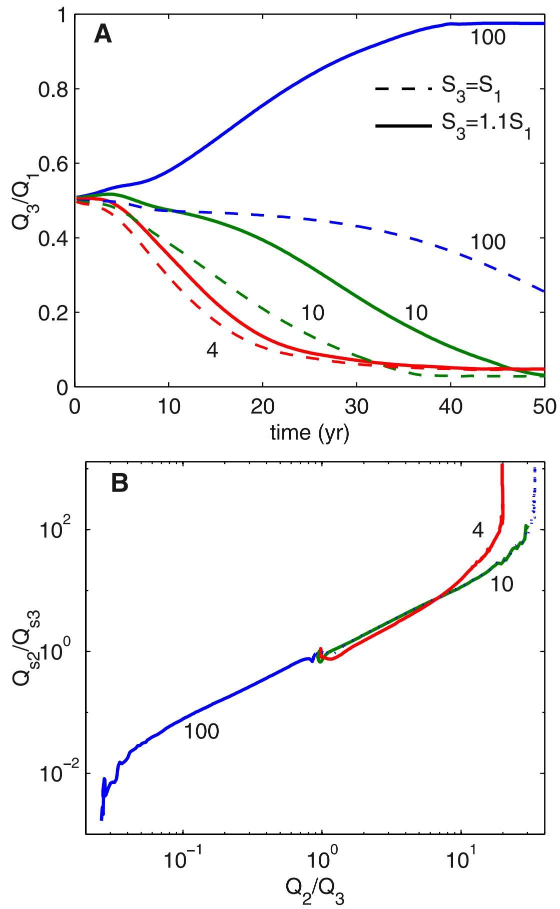

Figure 8. (a) Effect of increased gradient of the inner-bend bifurcate compared with cases with equal gradients (series 2 in Table 1). Time series of discharge for the inner-bend bifurcate ($S_2 = S_1$ and three-dimensional model in all cases). Also shown are the results for the fine grid with $R/W_1 = 4$. (b) Sediment and discharge division over the bifurcates for all runs shown in (a). The cases with $R/W_1 = 10$, 100 and $S_3 = S_1$ lie on top of the asymmetric case.

as in the one-dimensional model) the inner-bend bifurcate dominates for gentle bends ($R/W = 100$) whereas the outer-bend bifurcate dominates for sharper bends ($R/W = 10$). The nodal point relation remains similar to that in other runs (Figure 8b). In other words, a larger gradient (0–20%) in one bifurcate can be counteracted by upstream meander bend flow depending on the position of the steeper bifurcate along the meander. Hence combinations exist of bend radius and downstream gradients for which the bifurcation remains quasibalanced for a longer time.

4.3. Effects of Longer Bifurcates

[68] Avulsions are affected by their distance to the sea or lake relative to the backwater adaptation length. Four runs were done with extra long bifurcates (series 3 in Table 1): two were the normal model (with $L = 6$ km long bifurcates) extended to 31 km bifurcates (with $R/W_1 = 4$, 10), and the other two were extended to 106 km bifurcates (also $R/W_1 =$ 4, 10). The backwater adaptation length (at which the water level has adapted for 63%) can be estimated as $\lambda_{BW} \approx h/3S \approx 25$ km, so that the longest model is much longer than λ_{BW}. As presented earlier, the 6 km short bifurcates (connected to the upstream inner bend) silt up rapidly, particularly for a sharper bend. In contrast, the 31 km bifurcate silts up more slowly and the 106 km bifurcate aggrades much more slowly than the 6 km bifurcate with the same upstream bend radii (Figure 9a).

[69] The silting up apparently occurs in three distinct phases: (1) an initial bar formation phase in the upstream bend, (2) the stabilization of the bar pattern upstream of the bifurcation while the initial bars migrate through and out of the bifurcates, and (3) the gradual silting up of one bifurcate and erosion of the other. In the first phase (see Figures 7a and 9a: 0–10 year for 6-km long bifurcates; 0–20 year for 31 km long bifurcates with $R/W_1 = 10$) a bar migrates from upstream into the bifurcate which rapidly destabilizes the bifurcation (wiggles near $Q_2/Q_3 = 1$ in Figures 7b, 8b, and 9b). The bars were excited by the initial migrating alternating bars upstream of the bifurcation, and hence decayed when the upstream bend attained a near-equilibrium morphology, so that a finite train of about ten bars migrates through the bifurcates. The second phase is after 10 years for 6 km long bifurcates, after 20 years for 31 km long bifurcates, and not clearly distinguishable in the discharge division for 106 km long bifurcates. In this phase the train of bars migrates out of the bifurcates, which obviously takes

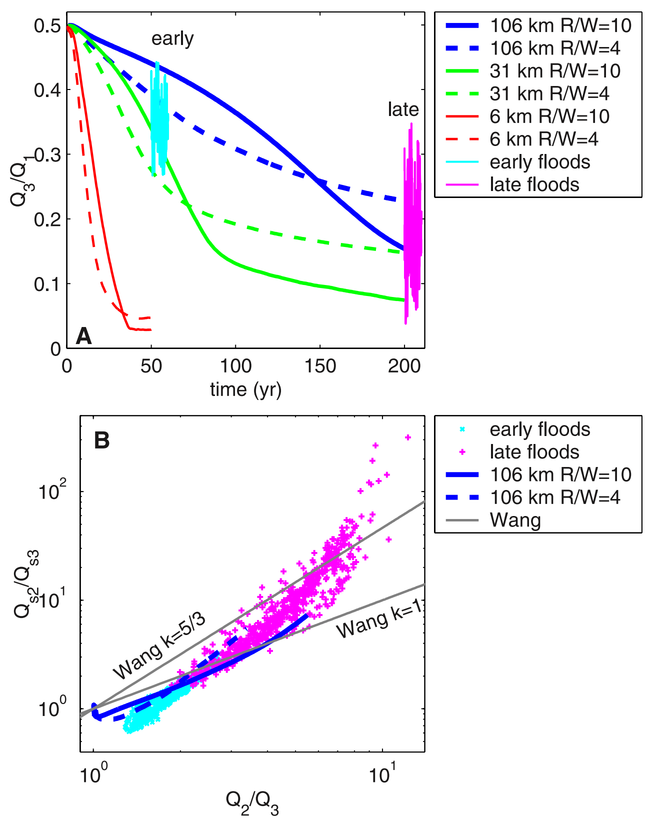

Figure 9. Effect of longer bifurcates ($R/W_1 = 4$, 10; series 3 in Table 1) and of natural discharge fluctuations (series 4) on the discharge division (a) and the sediment division (b). (a) Time series of discharge through the inner-bend bifurcate for various bend radii and bifurcate lengths. The natural discharge fluctuations (early after 50 years and late after 200 years) were applied to the 106 km, $R/W_1 = 4$ run. (b) Sediment division for the natural discharge fluctuations as symbols and as lines for the constant discharge.

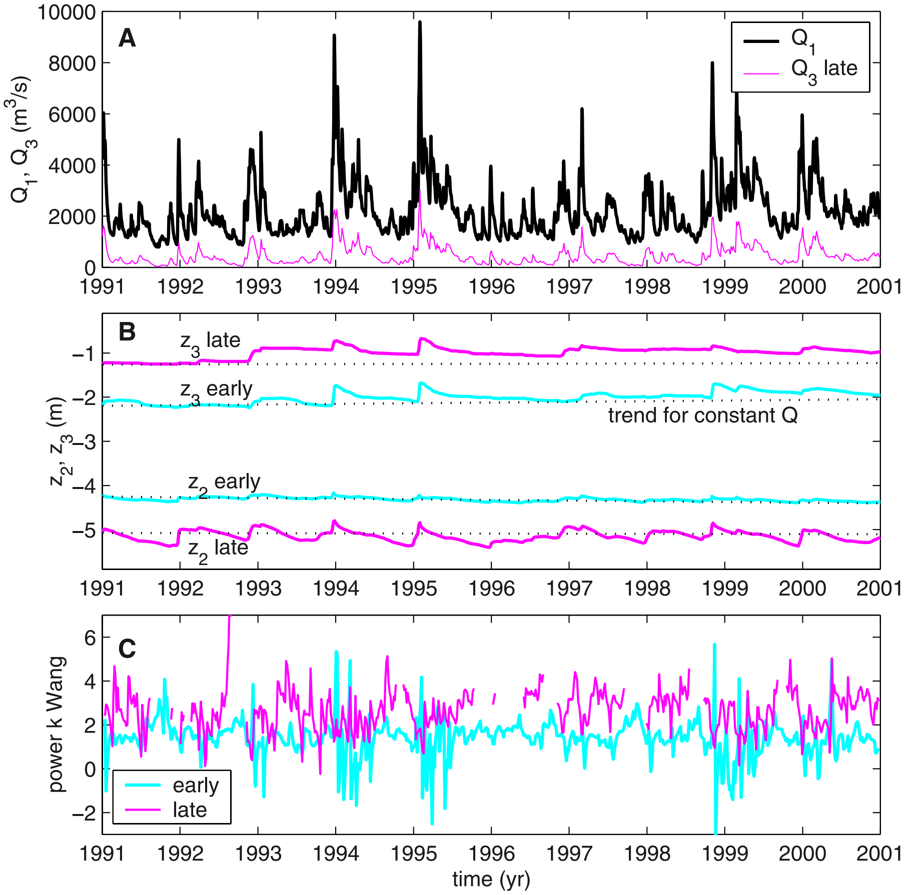

Figure 10. Effect of variable discharge (series 4 in Table 1) on the inlet step based on the discharge through the channel of the Rhine in 1991–2000 (minus overbank flow). (a) Time series of upstream and downstream discharge (inner-bend bifurcate, late run; see Figure 9 for timing). (b) Width-averaged bed levels at the entrances of the bifurcates for the early and late run (and also indicated for constant discharge). (c) Power k as defined by *Wang et al.* [1995] derived from the three-dimensional model results for early and late run.

a longer time in the longer bifurcates and has less effect because the length of the train relative to the bifurcate length is smaller. In the third phase (when Q_2 and Q_3 differ a factor of 5–20) the large upward bed slope into the closing bifurcate and the relative roughness become so large that sediment can no longer enter (Figures 6, 7b, and 9b) and the bifurcates stabilize.

[70] The runs with the long bifurcates clarify one aspect of the runs with the normal, short bifurcates: the difference in sediment division (Figure 9b). The sharper bends initially silt up more rapidly than the gentler bends, but their second phase commences much earlier so that eventually the silting up occurs more slowly than in the gentler bends. In phase 1 $k \geq 1$ whereas in phase 2 $k \geq 5/3$. This higher power occurs early in the sharper bend runs because the bend effect on the flow and sediment division is stronger so that it initially deviates more from $k = 1$.

4.4. Effect of Varying Discharge

[71] In the model results presented so far, the discharge was constant at (Q = 2500 m^3/s). At this value the same amount of sediment is transported annually as for the complete discharge record of the past century. It was assumed that floods did not significantly affect bifurcation evolution, because the morphological adaptation timescale of the entire closing bifurcate is of the order of decades (depending on bifurcate length) whereas a flood takes place within a month. Hence feeding the model with this constant discharge or feeding it with the discharge record would not result in very different large-scale morphology of a single branch (given absence of bank erosion/accretion). However, the variable discharge might affect the local bar development at the bifurcation, and since the bifurcation evolution is affected by local bars this must be investigated.

[72] As a realistic boundary condition, a time series of discharge through the channel of the Rhine in the period 1991–2000 was specified for the R/W_1 = 4 run with 106 km long bifurcates. This discharge record (Figure 10a) is just used as an exemplary natural time series and the roughness length is kept constant. This particular model run with long bifurcates ($>\lambda_{BW}$) was chosen because the specified downstream water levels are far away from the bifurcation so that using a constant water level rather than a stage–discharge relation, which is unknown, does not affect the flow in the vicinity of the bifurcation. It is computationally too expensive to run the model for 200 years without the morphological multiplication factor. Therefore the time series was applied to the morphology calculated for constant discharge

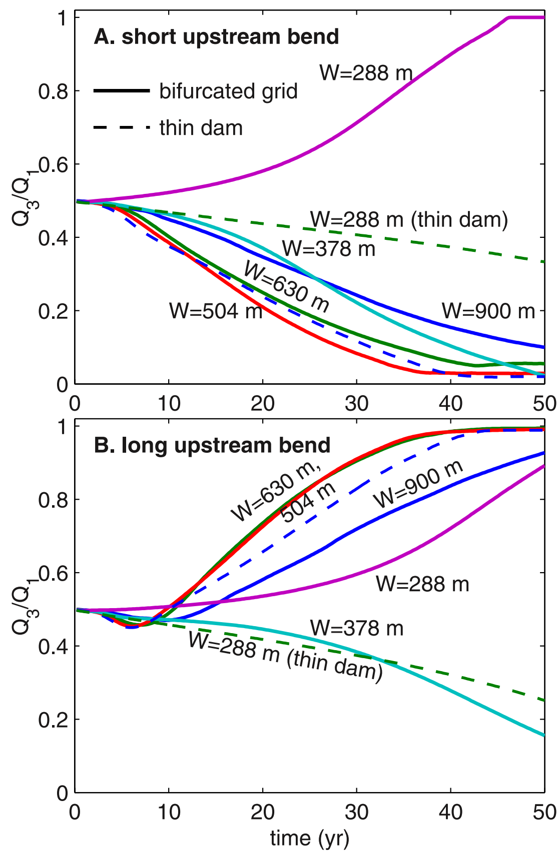

Figure 11. Effect of channel width on the discharge division over time (all bends have R/W_1 = 10). (a) Short upstream bend (series 5 in Table 1). (b) Long upstream bend (series 6).

(discussed in the previous section) in two stages of the bifurcation evolution: after 50 (hereafter called "early") and after 200 years ("late") of constant discharge (Figure 9a and series 4 in Table 1).

[73] The late run shows larger discharge fluctuations than the early run (Figure 9a). While the minor bifurcate gradually closes off in terms of rising bed levels and decreasing average discharge, it continues to experience large floods and hence a more "flashy" discharge regime. The discharge peaks lead to increased inlet step heights, in particular for the late run, but this is partly counteracted by erosion immediately after the discharge peak (Figure 10b). The net effect of discharge variation in contrast to constant discharge is nearly negligible. Only for the late run with its larger discharge fluctuations the closing bifurcate silts up more rapidly ($\approx$0.01–0.02 m/a), because the floods cause higher water levels at the bifurcation, leading to a more symmetrical flow division, more sediment supply and less flow deceleration in the closing bifurcate.

[74] The power k of the *Wang et al.* [1995] nodal point concept was derived from model results by fitting a power function through the sediment transport (dependent variable) and discharge ratios (independent) in a window of five time steps moved along the entire time series. The k for the natural discharge series is highly variable, with peaks at low discharge when the steps become more pronounced, and dips at peak and falling discharge when the steps are eroded (Figure 10c). As expected, at high discharges the water depths in both bifurcates increases and becomes more equal, so that the sediment can also be divided more equally (depending on the preflood morphology). Plotted as a nodal point relation (Figure 9b) this causes scatter on otherwise fairly similar trends of the sediment division as a function of discharge division. In other words, floods do not significantly affect the bed evolution of model bifurcations compared with other effects studied in this paper. We obviously ignore bank erosion and floodplain processes for which floods are important in real bifurcations as will be discussed later.

4.5. Effect of Width–Depth Ratio and of Upstream Bend Length

[75] In section 2.3 an effect of width–depth ratio on the bar dynamics was predicted, and as a consequence of this an additional effect was predicted of the location of the overshoot, which is here determined by the distance between the bifurcation and the beginning of the bend, which acts as the perturbation that generates the steady alternate bars. The results are compared with bends without bifurcations.

[76] The effect of the width–depth ratio on the discharge division and overall bifurcation morphology in the three-dimensional model results is dramatic (Figure 11 and series 5 in Table 1): between W = 288–378 m the bifurcation switches from a dominant inner-bend bifurcate to a dominant outer-bend bifurcate.

[77] The effect of the length of the upstream bend (see Figure 3 middle compared to with top) is also quite dramatic (series 6 in Table 1). The dominant bifurcates for W_1 = 504 and 630 m are switched from the outer to the inner bend. The widest channel (W_1 = 900 m) also develops in the same direction, but slower than the narrower channels. For the narrower channels the results are less clear, particularly when compared with the alternative schematization of bifurcations by a thin dam (Figure 3 bottom grid, see discussion). For the 288 m wide channel the inner-bend bifurcate always dominates, which is due to a scour hole in that bifurcate just downstream of the bifurcation which attracted the flow. A similar scour hole also developed initially in the inner-bend bifurcates with larger widths (also see Figure 6) but was quickly removed there by the inner-bend bar extending from the upstream bend into the inner-bend bifurcate, leading to a dominant outer-bend bifurcate in all cases. This indicates that the bifurcation behavior "bifurcates" at a certain width 288 < W < 378 m (but see the sensitivity analysis on the model schematization) due to bar behavior differences for different width/depth ratios as explained further below. This contrasts to the switching behavior of a certain bend radius combined with a gradient advantage of the inner-bend bifurcate (Figure 8a) which may happen for arbitrary width–depth ratios given enough additional gradient.

[78] To further illustrate the effect of bar behavior on the change of direction in bifurcation evolution, longitudinal profiles near the outer-bend bank are shown in Figure 12 (short bends on the left hand side, long bends on the right). The results illustrate the switch of dominant channel and the underdamped to unstable bar behavior for increasing channel width. For comparison to the case without the bifurcation, additional runs were done of bends without bifurcations with a straight downstream section (Figure 13 and series 7 in

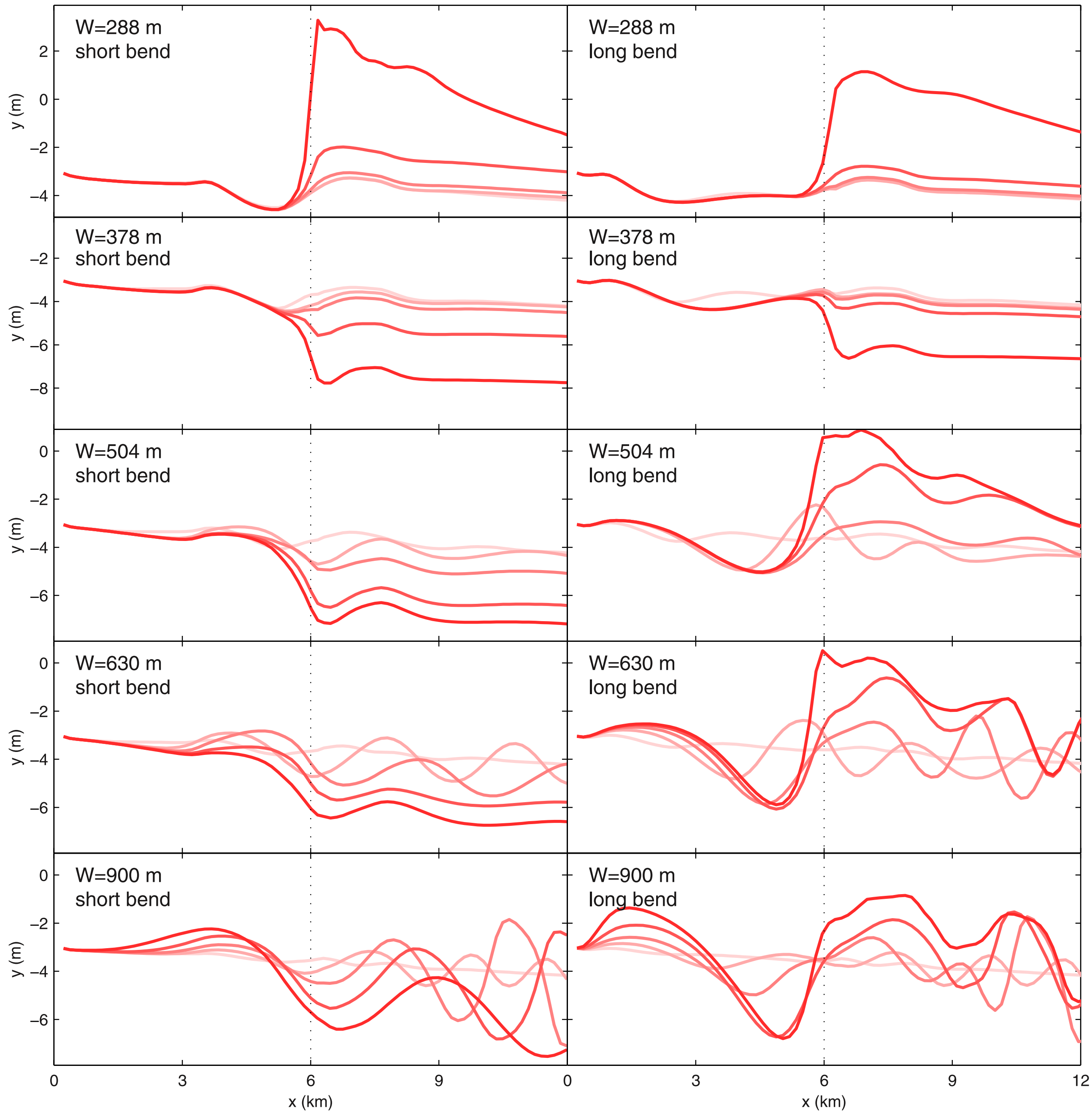

Figure 12. Long profiles for standard bifurcation grids of the bed level at the right bank (in the outer bend of the upstream branch and into the right bifurcate) at various times for bifurcations of various channel widths (top to bottom). (left) Short upstream bends (series 1 in Table 1). (right) Long upstream bends (series 6). The bifurcation is at exactly 6 km, and the flow is from left to right. The shades from light to dark indicate 1.6, 6.4, 12.7, 25.3, and 50 years (R/W_1 = 10).

Table 1). An alternative schematization of bifurcations by a thin dam (Figure 13 and series 8 in Table 1) will be discussed later.

[79] The 288 m wide bends have fairly damped bar dynamics as predicted (Figure 13, top four panels). The longer bend clearly shows more of the overshoot phenomenon with a deep pool and high bar superimposed on the overall bend morphology. The 504 m wide bends (Figure 13, bottom four panels), on the other hand, show unstable growing bars that increase in wavelength while migrating downstream. For the long bend this starts further upstream than for the short bend, so that a bar top is present in the outer bend at the location of the bifurcation, whereas the short bend has a bar trough at the same location. This explains the difference between the bifurcation with W = 504 m and a short or long bend (Figure 12): the outer-bend bifurcate in the short-bend run is initially deepened by the bar trough whereas it is aggraded by the bar top in the long-bend run.

[80] The second bar top in the bend model (Figure 13, long bend with W_1 = 504, top right in the graph) shows nonlinear effects of small water depth by its sharp point and

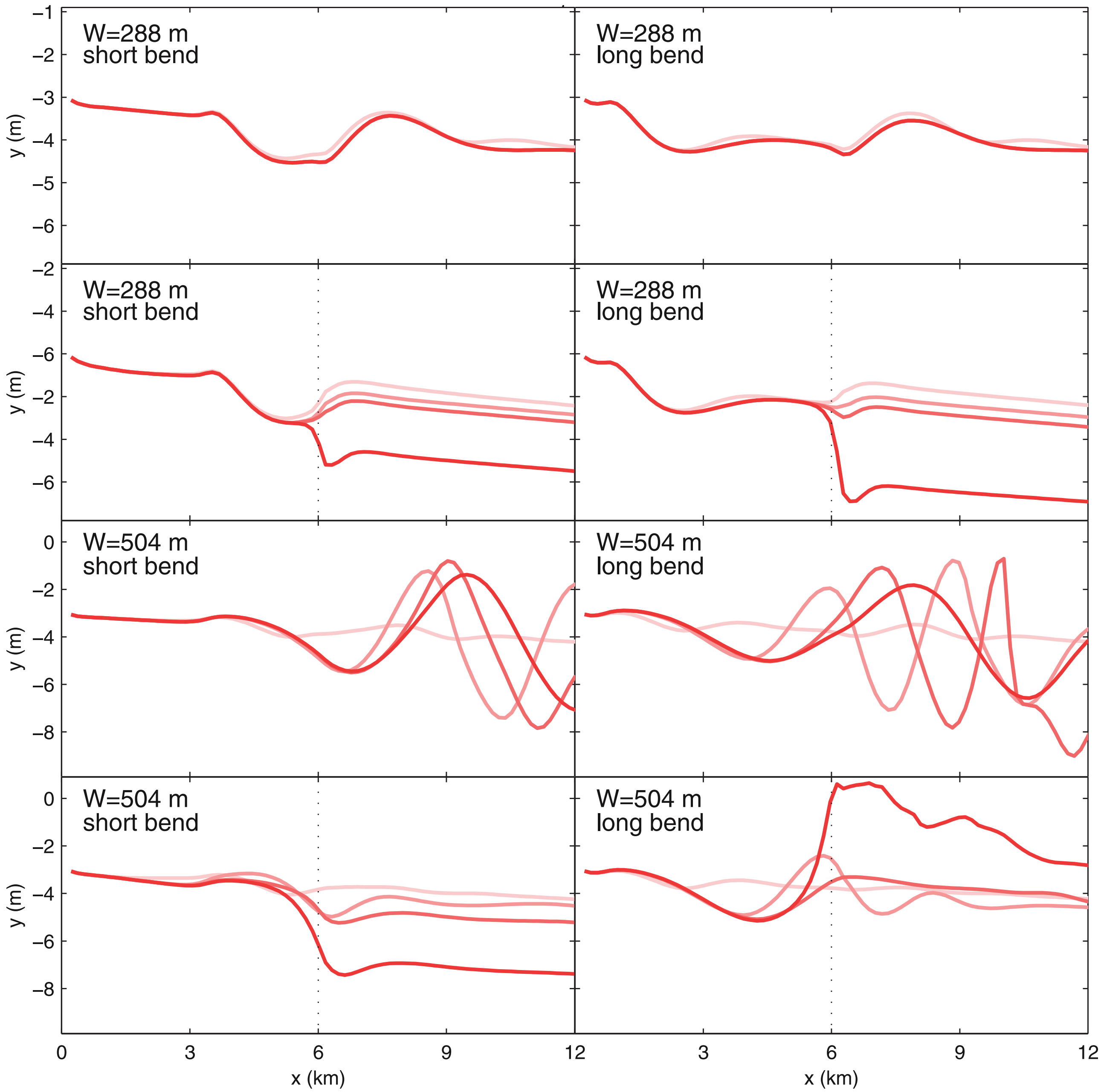

Figure 13. (left) Long profiles for short bends without bifurcations (series 7 in Table 1) and with bifurcations schematized as bends with a thin dam along the second half (series 8). (right) The same, with long upstream bends. Bed levels are at the right bank (in the outer bend of the upstream branch) at various times for two bifurcations with short and long upstream bends (downstream sections is straight). The bifurcation is at exactly 6 km (indicated by dashed line) and the flow is from left to right. The shades from light to dark indicate 1.6, 6.4, 12.7, 25.3, and 50 years (R/W_1 = 10). Compare with Figure 12.

shorter length. Such effects are also clear in the nearly closed bifurcates. The profiles of the very shallow bifurcates are irregular because a braided pattern is developed due to the large width–depth ratios.

[81] For the runs with the extra long bifurcates the bar evolution (not shown) is very similar to their short-bifurcate counterparts. The growing bars migrate into the bifurcates where they stabilize their wavelength at about 4 km and gradually migrate out of the model domain.

[82] Finally, the transition from the bed level in the upstream channel to the bed levels in the bifurcates takes place just upstream of the bifurcation over a length of about 1–2 W_1 in agreement with the assumption by *Bolla Pittaluga et al.* [2003]. This upstream influence is present in very narrow and very wide upstream branches alike regardless of the bar damping (Figure 12).

5. Sensitivity Analysis

[83] In this chapter we present the sensitivity of our results (series 9–12 in Table 1) to various choices in the model schematization, namely the roughness formulation,

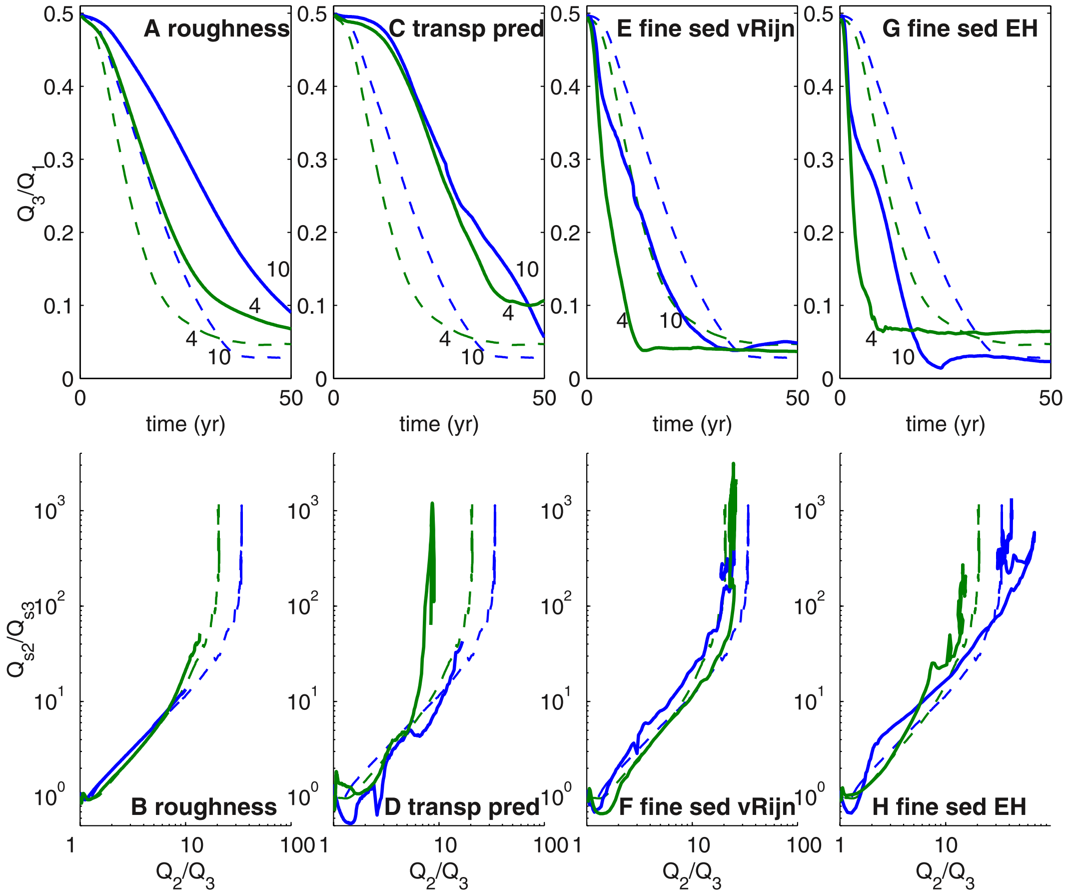

Figure 14. Sensitivity analysis of model results. (a, c, e, g) Time series of discharge for the inner-bend bifurcate. Labels indicate R/W_1: bend radius R as a multiple of the upstream channel width W_1. (b, d, f, h) Sediment and discharge division over the bifurcates. The thin dashed lines (in all subfigure s) are the standard runs with *Engelund and Hansen* [1967], Darcy-Weisbach roughness with k_s = 0.15 m and D_{50} = 2 mm sediment (series 1 in Table 1). (a, b) The effect of using a constant Chézy roughness (series 9). (c, d) The effect of using *Van Rijn* [1984a] (series 11). (e, f) The effect of using fine sediment (D_{50} = 0.5 mm) and *Van Rijn* [1984a] (series 13). (g, h) The effect of using fine sediment (D_{50} = 0.5 mm) and *Engelund and Hansen* [1967] (series 10).

the grain size and the sediment transport predictor. Moreover, results from a different type of bifurcation grid are compared with the standard grid results presented above (series 8).

5.1. Sensitivity to Roughness, Grain Size and Transport Formulations

[84] In this section a number of extra tests are presented to indicate the sensitivity of our results to choices of roughness formulation (series 9 in Table 1), grain size (series 10 and 12 in Table 1) and the transport formulation (series 11 and 12 in Table 1). These tests were all done with the "standard" 12 km long grids with short bifurcates and short upstream bends of 4 $W < R < 10$ W (Figure 14).

[85] Runs with a constant Chézy roughness value rather than a constant Nikuradse roughness length led to longer timescales (Figure 14a), but the nodal point relation was very similar in that it shows the same three distinct phases: same initial fluctuations, period of constant power k and the same near-closure behavior of highly increasing Q_{s2}/Q_{s3} for a nearly constant Q_2/Q_3 (Figure 14b). The constant Chézy roughness (1) damps the underdamped bars more than with constant roughness lengths, (2) causes the bars to migrate downstream more slowly, and (3) causes the asymmetry of bed levels of the bifurcates to develop more slowly. This agrees with the expected behavior based on the equations, because L_D is inversely proportional to C while C (using a constant Nikuradse roughness length) varies with water depth. So when a bar develops, the water depth above it is decreased and for constant Nikuradse roughness this results in a smaller C, which then increases L_D and consequently amplifies the bar behavior.

[86] It takes longer before morphological equilibrium is reached if the *Van Rijn* [1984a, 1984b] sediment transport predictors are used instead of the *Engelund and Hansen* [1967] predictor (Figures 14c and 14d). The nodal point relation was similar to the standard settings (but more erratic) in that it shows the same three distinct phases. However, the morphology was different in two aspects. The amplitude of the bars was much larger. This was partly due to the problem that the *Van Rijn* [1984a, 1984b] sediment transport predictors in the Delft three-dimensional system contain a hard threshold for the initiation of motion, which strongly affects shallow bars, but also due to the absence of

a correction for slope effects in the relations for transport rate and critical shear stress. Hence the alternating bars increased in height relative to the model runs with the *Engelund and Hansen* [1967] predictor, and, moreover, deep scours developed near the opposite bank. Similar behavior was observed for some runs with the *Meyer-Peter and Mueller* [1948] predictor (not shown). The deep scour and very high bars caused the more erratic result of the sediment division, which we therefore attribute to the missing slope effects with this sediment transport predictor and its sensitivity to slope effects and incipient motion.

[87] When the grain size is decreased to D_{50} = 0.5 mm, the morphology reacts much faster due to the higher sediment mobility (Figures 14e–14h). Hence the bifurcation destabilizes much faster and at smaller Q_2/Q_3 ratios. The models were also run for the combination of fine sediment and the *Van Rijn* [1984a, 1984b] predictor for comparison to the *Engelund and Hansen* [1967] predictor with the same fine sediment. In these runs the sediment was more mobile than in the standard sediment with $\theta \approx 0.5$ and the suspended sediment transport rate was two to three times as large as the bed load transport rate.

[88] The transverse slope in the bends is larger for the finer sediment, and the wavelength of the bars is slightly larger. The nodal point relation of the *Van Rijn* [1984a, 1984b] predictor (Figures 14e and 14f) with the fine sediment (in contrast to that with the coarse sediment) is within a factor of 2 of the nodal point relation with *Engelund and Hansen* [1967] with the coarser sediment. The better agreement between the two predictors, despite the difference in sediment size, is because the aforementioned problems in the work of *Van Rijn* [1984a, 1984b] with critical shear stress on slopes is less relevant in the fine sediment. However, the results with the work of *Engelund and Hansen* [1967] and the fine sediment (Figures 14g and 14h) are less satisfactory (more irregular), which is due to the very high sediment transport rates. This could be improved by changing the entire model setup with smaller time steps and other adaptations, but this is outside the scope of the present paper.

[89] Despite the problems with predictors with a threshold of motion and with high transport rates it is clear from this and other experiences that the overall behavior of the bifurcation and the trend of the nodal point division remains similar, even if a different roughness formulation or sediment transport predictor leads to somewhat different bar dynamics and morphological timescales. Using different sediment transport predictors the timescale of adaptation of Q_3/Q_1 is within a factor 2, which is entirely reasonable given the uncertainties of the predictors. Nevertheless, bifurcations at sensitive combinations of downstream slope advantage and upstream bend radius are very sensitive to bar dynamics at the bifurcation, such as those with upstream channel widths of 288–378 m. In such critical conditions a different roughness formulation or sediment transport predictor (and/or slope effects) would give great uncertainties in the direction of evolution of the bifurcates. The inherent unpredictability of bifurcations will be discussed later.

5.2. Sensitivity to Bifurcation Schematization

[90] Below we present some tests to ascertain the sensitivity of our results to the chosen schematization of the bifurcation (series 8 in Table 1). These tests were all done with the “standard” 12 km long grids with short bifurcates and short upstream bends of 4 $W < R <$ 100 W (Figure 3 top). The schematization of the bifurcation used so far has a bluff facing the flow at the bifurcation. The grid cells are defined by the nodes (corner points of the cells). To bifurcate the flow and sediment transport, one row of nodes has to disappear. As that row provides the corner points to two adjacent rows of cells, a strip of two cells wide disappears from the grid (see middle inset in Figure 3). The resulting bluff may have affected our results.

[91] An alternative way to define a grid with a bifurcation in the Delft three-dimensional system is by specifying a thin dam on the centerline of the second half of a bend, which splits the channel laterally into two channels (Figure 3 bottom). This has the advantage that all nodes remain active, contrary to the standard bifurcations in this paper, so that the upstream channel does not have to be widened and the cells of the downstream channels do not have to be widened. Hence differences between this schematization and the standard bifurcated grids can be ascribed to the differences in bluff width and channel widening upstream of the bifurcation. The disadvantage of this grid is that the bifurcates cannot be given different directions which makes it less applicable for practical applications.

[92] Several model runs with thin dams and short bends with R/W_1 = 4–100 were compared with the runs presented above, and found to give very similar results for W = 504 m (see Figure 11 for discharge and compare Figures 12 and 13 for morphology). The bar patterns are also very similar. However, for W = 288 m the thin dam bifurcations differ from the standard bifurcations (Figure 11): the opposite bifurcate dominates. In fact, the thin dam bifurcations behave as expected: the same bifurcates dominate as for wider channels and the adaptation time is longer because the closure of one bifurcate is not accelerated by an unstable bar as in the wider runs. The standard bifurcations with W = 288 m, on the other hand, developed scour holes just downstream of the bifurcation which attracted so much flow that the opposite bifurcate was kept open. This scour hole was not developed in the thin dam models.

[93] These results mean that the bifurcations with narrower channels presented in this paper are sensitive to the manner in which the bifurcation grids have been schematized. However, the general conclusions remain valid: at certain combinations of upstream bend radius and downstream slope advantage of the inner-bend bifurcate, these two effects cancel out so that the bifurcation remains quasistable. The model runs are obviously the most sensitive to initial and boundary conditions and schematization near the critical combinations where bifurcations are quasibalanced.

6. Test of Nodal Point Concepts With Three-Dimensional Model Results

[94] We first compare the division of flow discharge and of sediment transport as derived from the three-dimensional model results to those calculated by nodal point relations for sediment division based on the flow division from the three-dimensional model results. This will be used to test the underlying assumptions of the nodal point relations. Then we present results of one-dimensional model calculations of morphodynamics with the new nodal point relation for some bifurcations where the upstream bend and a downstream

slope advantage compete, and compare these results to the three-dimensional model results for an integral evaluation of the one-dimensional model concepts embedded in a one-dimensional model.

6.1. Division of Flow Discharge

[95] One important parameter determining the deflection of the sediment transport is the angle of the shear stress. In the *Bolla Pittaluga et al.* [2003] concept this angle is based on the ratio of depth-averaged streamwise to transverse flow velocity u/v. The transverse flow velocities calculated by the three-dimensional model are shown in Figures 15 and 16. The model results show some transverse flow due to the bends, but most prominently in the zone 1–2 km upstream of the bifurcation. More importantly, the bend morphology shows the overshoot phenomenon with a deeper scour and higher shoal at the entrance of the bifurcation compared with further downstream (Figures 15a, 15e, 15f, and 15j). The high shoal obviously reduces the flow through this bifurcate. The overshoot is not incorporated in the one-dimensional concept so that the bifurcate may be expected to silt up less fast and perhaps not at all.

[96] The transverse discharge as defined in the nodal point concepts was derived from the model results as follows. The true transverse discharge was calculated with equation (2) from discharges through cross-sections in the three branches in the three-dimensional model. The transverse discharge and sediment transport were also derived from the model results over the midchannel line of $0-1W_1$ upstream of the bifurcation ("local" in Figure 17) and over the full length of the upstream branch ("all" in Figure 17). The latter need not be exactly the same because the model adjusts the distribution of discharge over the upstream boundary depending on the morphology.

[97] Within the first 10 years (phase 1), the bed adapts rapidly to the bend flow (Figure 17a) while the flow divides over the bifurcates at $1-2$ W_1 upstream of the bifurcation (Figures 15 and 16). The deviations from a simple symmetrical flow division (given that $W_2 = W_3$) are caused by the bed adaptation and initial bars. Later the discrepancy between the true Q_y and the local Q_y (across the channel centerline with length 1 W_1 upstream of the bifurcation) increases (Figure 17a). This is due to the three-dimensional bar pattern just upstream of the bifurcation including that associated with the overshoot phenomena, and due to the redistribution of flow that took place further upstream (Figure 15b) after the bed adapted to the downstream closing bifurcate (Figures 15h, 15i, and 15j). Hence the deviations are partly the result of the artificial development of bend-related morphology from an initially plane bed upstream of the bifurcation, while the one-dimensional concept assumes an equal distribution of specific discharge over the cross-section upstream (equation (2)) and partly from the dynamics caused by the presence of the bifurcation, which are difficult to separate. In short, deviations between the local transverse flow discharge in the one-dimensional concepts and in the three-dimensional model are considerable and will cause deviations in transverse sediment flux.

6.2. Division of Sediment Transport

[98] In the one-dimensional nodal point concepts the transverse sediment flux depends on the transverse flow discharge (and the transverse bed slope and spiral flow). To test the transverse sediment flux parts of the one-dimensional nodal point concepts independently of the discharge division parts (which were shown above to deviate from the three-dimensional model results), the transverse sediment flux calculation done below will be based on transverse flow and bed levels from the three-dimensional model. The transverse sediment flux Q_{sy} is extracted from the three-dimensional model runs across the centerline upstream of the bifurcation. This was done over a length of 1 W_1 ("local") or alternatively over the full length ("all") of the upstream branch, the same as for transverse flow discharge discussed above. The water depths and bed levels in the three-dimensional model were averaged over areas per branch just upstream and downstream of the bifurcation over the full widths of the bifurcates and over lengths of 1 W_1.

[99] Several comparisons between the three-dimensional model and the nodal point relations are shown (Figure 17). For $R/W_1 = 10$, the transverse sediment flux according to the *Bolla Pittaluga et al.* [2003] concept is nearly a factor of two too large (Figure 17b, full lines) compared with the three-dimensional model results, whereas the new relation (equation (27)) overpredicts by a factor of 1.5, indicating that including the spiral flow improves the nodal point relation. However, the three-dimensional model with the gentle bend has a poorer agreement than with sharper bends (Figure 17d), demonstrating that the transverse sediment flux is not only affected by the spiral flow but also by the three-dimensional bar pattern.

[100] The predictions of transverse sediment flux by the concept agree better with the full transverse flux in the three-dimensional model across the entire centerline ("all", dashed in Figure 17b), but then the initial predictions are poor (offset) because the flux in the three-dimensional model results include the initial sediment redistribution to adapt the bed to the bend flow. This demonstrates that the true upstream region of influence where transverse flow and sediment fluxes affect the divisions at the bifurcation is longer than $1-3$ W_1. One could argue that this is entirely due to the upstream redistribution of flow over the width and not due to the transverse sediment flux. Indeed, the results further improve when the ("local") transverse flow discharge across the 1 W_1 centerline of the three-dimensional model is used (instead of the "true" transverse flow) for the nodal point relations rather than the entire ("all") transverse discharge derived from the flux through the bifurcates (Figure 17c). However, even then the agreement is still not perfect which reflects the deviations between the three-dimensional model and the nodal point relations due to the combination of three-dimensional flow and bar patterns in the entire bend upstream of the bifurcation.

6.3. Comparison of One-Dimensional and Three-Dimensional Models

[101] In practice, one-dimensional nodal point relations will be embedded in one-dimensional models, so we will now compare the three-dimensional model results to one-dimensional model results with the new nodal point relation (Figure 18).

[102] The one-dimensional nodal point relation has two relevant parameters that can be calibrated: ε and α_W. The spiral flow intensity at the bifurcation node depends linearly on the calibration parameter ε (equation (12)). The trans-

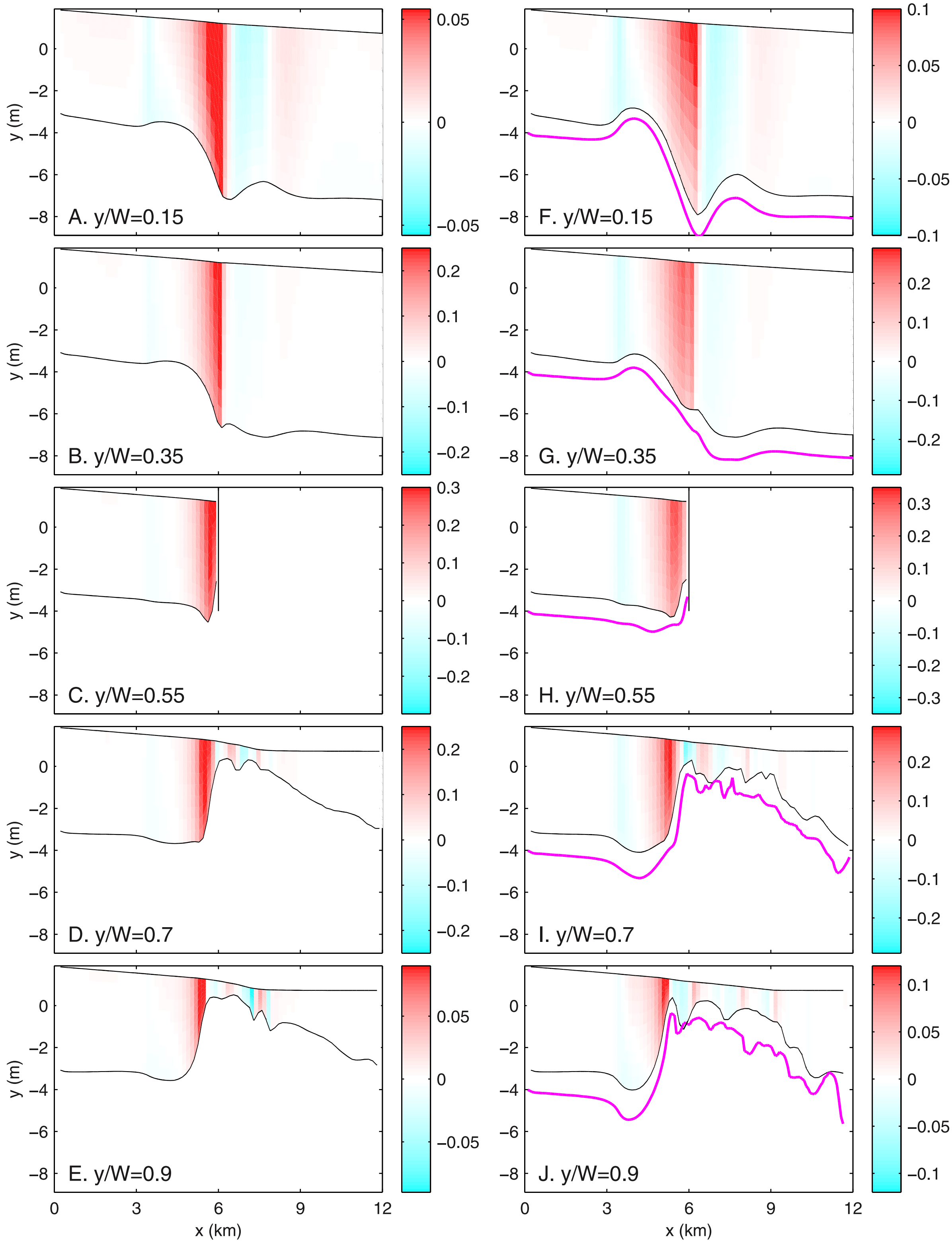

Figure 15. The transverse flow velocity (scale in positive m/s toward right bank) for several sections along the entire model (position in fractions of W from right bank) after 50 years model time (short upstream bend; series 1 in Table 1). (a–e) $R/W_1 = 10$. (f–j) $R/W_1 = 4$, bed level of fine alternative grid given with offset of -1 m. The bifurcation is at exactly 6 km, and the flow is from left to right.

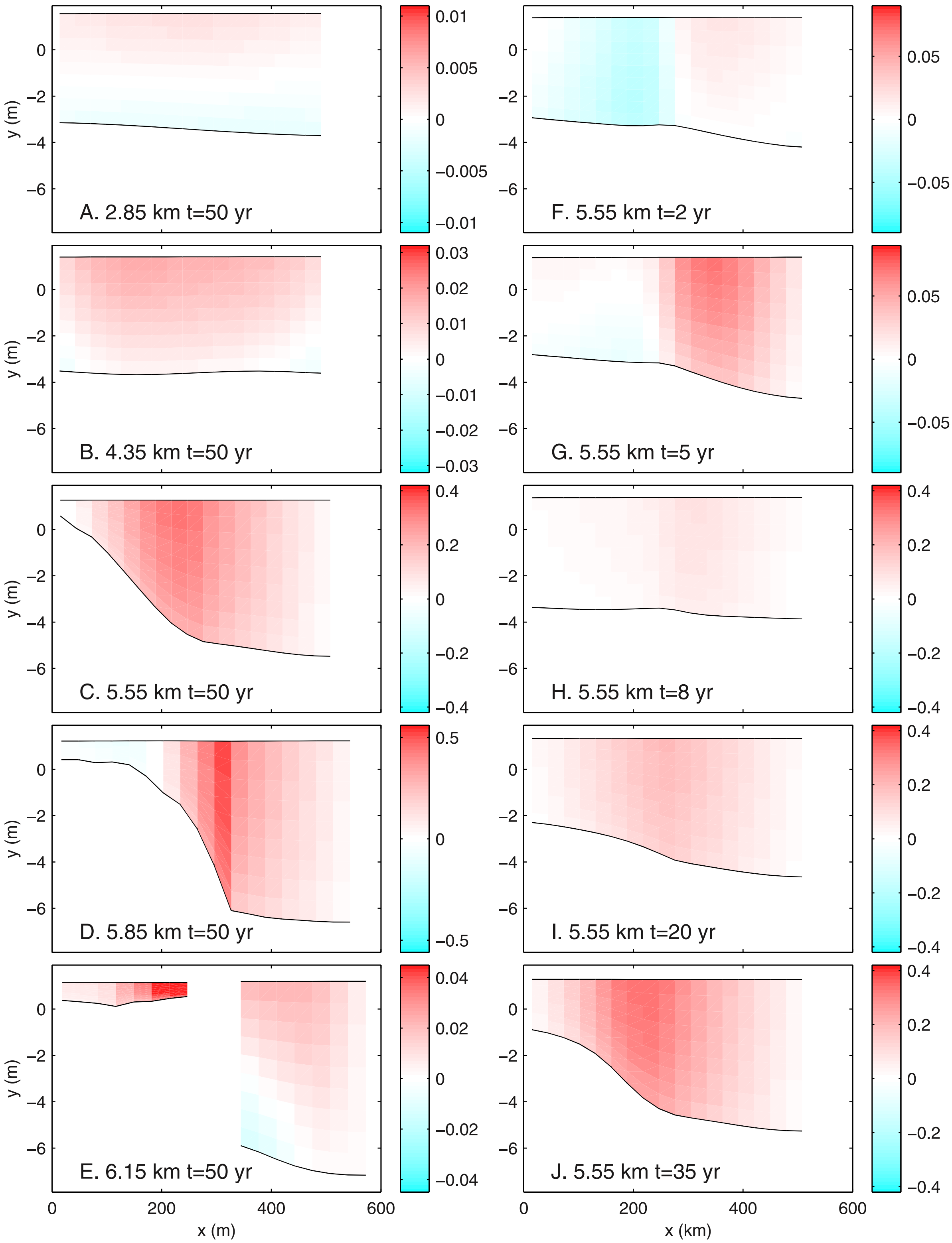

Figure 16. The transverse flow velocity in R/W_1 = 10 (scale in positive m/s toward right bank) for several cross-sections (position in km from upstream boundary; bifurcation is located at 6 km) upstream and just downstream of the bifurcation after 50 years model time (a–e) and for various times (f–j) in the cross-section shown in c (short upstream bend; series 1 in Table 1).

verse component of the sediment transport depends on the angle of the shear stress vector (equation (11)) and on the ratio v/u, which is inversely related to the second calibration parameter α_W. Thus ε and α_W each determine the effect of the bend radius or slope, respectively, and together they determine how the bend and slope effects are balanced. In the three-dimensional model, $\varepsilon = 1$ and in the work of *Bolla Pittaluga et al.* [2003] $\alpha_W = 1$. However, in the one-dimensional model this parameter setting leads to a much larger final discharge of the smaller bifurcate than in the three-dimensional model although the general model behavior is the same for both settings. The results with $\alpha_W = 3$ (extended length scale of transverse fluxes) and $\varepsilon = 2$ (stronger spiral flow) are more similar to the results of the three-dimensional model for the river Rhine (Figure 18). These larger, calibrated values are necessary to compensate for the lack of overdeepening effects in the one-dimensional model and for the deviation between the modeled and nodal point sediment divisions.

[103] For further comparison the previously published nodal point relations were also applied in the one-dimensional model. Obviously, the *Wang et al.* [1995] and *Bolla Pittaluga et al.* [2003] nodal point relations do not account for upstream bends but only give a changing discharge division when one of the bifurcates has a larger slope (Figure 18d). For small k, the *Wang et al.* [1995] relation does not lead to stabilization of the discharge but leads to full closure (just before which the simple one-dimensional model crashes), whereas the *Bolla Pittaluga et al.* [2003] relation stabilizes the bifurcation (at a highly asymmetrical discharge division) due to the feedback by the transverse slope effect.

[104] Summarizing, the new nodal point relation behaves qualitatively similar to the three-dimensional model which is of use for one-dimensional models applied to geological timescales. However, there are large quantitative differences in the initial stages, the adaptation path to equilibrium and the equilibrium attained due to the complexities present in the three-dimensional model but absent in the one-dimensional model. The initial differences are due to the formation of local bars and scour at the bifurcation in the three-dimensional model. The differences in adaptation and final equilibrium discharge division are caused by the three-dimensionality of the flow and the bed (local bars and scour at the bifurcation, and nonlinear transverse bed slopes) in the three-dimensional model, and the adaptation of the spiral flow to the local bed rather than assuming equilibrium spiral flow for infinite ideal bends as in the one-dimensional model. These phenomena clearly need more study to improve the new nodal point relation but for the

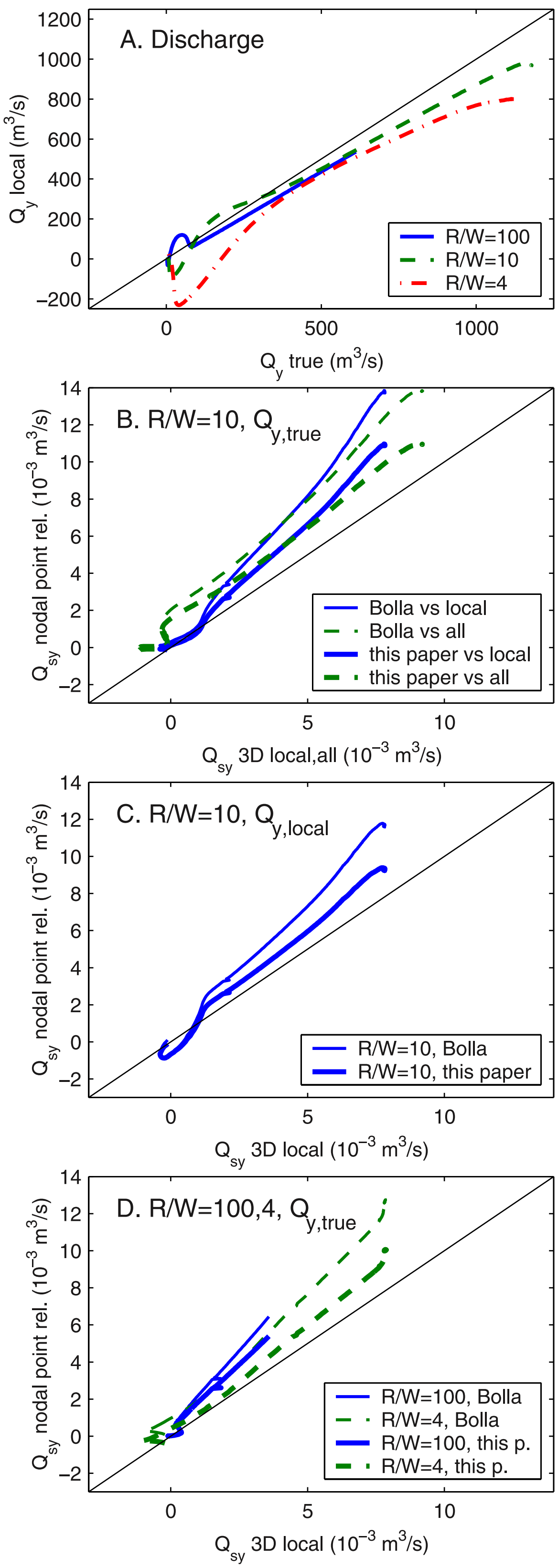

Figure 17. Comparison of the transverse flow (a) and sediment discharge (b–d) of the one-dimensional nodal point relations compared with the three-dimensional model (series 1 in Table 1). $\alpha_W = 1$ in the nodal point relations. The thin line indicates perfect agreement. The lines indicate an evolution in time from the lower left to the upper right corners. "Local" indicates the transverse flux over the midchannel line between 0 and $1W_1$ upstream of the bifurcation; "all" indicates the same over the full length of the upstream channel. $Q_{y,\mathrm{true}}$ indicates the true transverse discharge as determined from the integrated fluxes through the bifurcates whereas $Q_{y,\mathrm{local}}$ is the discharge across the midchannel line between 0 and $1W_1$ upstream of the bifurcation.

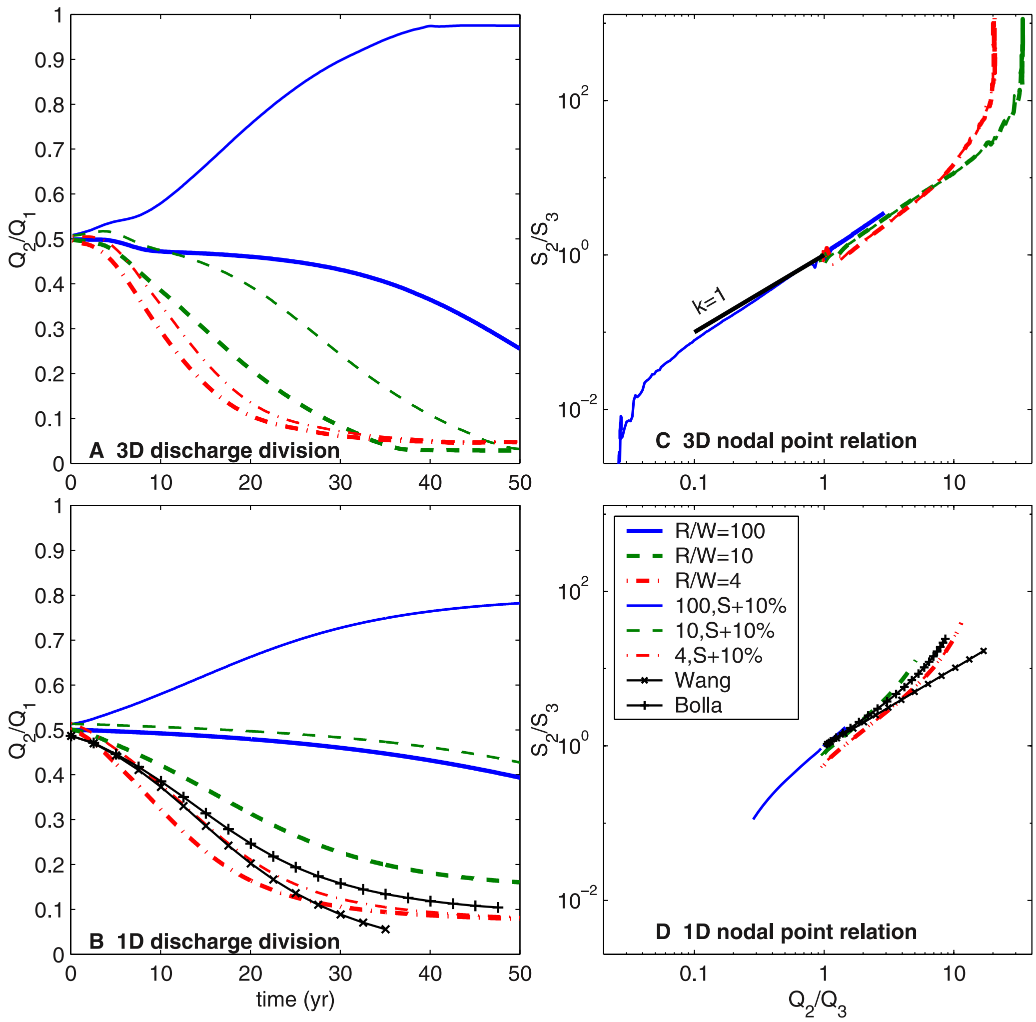

Figure 18. Comparison of three-dimensional (a and c; series 1 and 2 in Table 1) and one-dimensional model (b, d) results. The effect of a bend on the discharge division evolution is shown (a, b), as well as the added effect of a larger slope of the bifurcate connected to the inner bend. The nodal point relation (sediment division) (c, d) is shown in contrast to that by *Wang et al.* [1995] and *Bolla Pittaluga et al.* [2003], neither of which include effects of an upstream bend.

present analysis of general behavior it is sufficient that the results of the one-dimensional and three-dimensional models are qualitatively similar.

7. Discussion

[105] First we discuss the effects of bar dynamics just upstream of the bifurcation and implications for predictability of bifurcation evolution. Next some assumptions are evaluated that underlie nodal point relations for one-dimensional models, and future directions for further research on nodal point relations and bifurcations are suggested.

[106] Then we discuss the wider implications of our results for bifurcation stability and avulsion duration in the real world. The potential effects of sediment mixtures in the channel bed and of interactions between channels and floodplain are assessed. The reasons for the existence of residual channels and anastomosing rivers are reinterpreted based on the model results. Finally future directions for research on bifurcations are suggested.

7.1. Bar Dynamics and Limited Predictability of Bifurcation Evolution by One-Dimensional Models

[107] We have shown that bifurcations may be very sensitive to the local bar dynamics. In particular, underdamped bars in the upstream channel considerably affect the division of flow and sediment. It is possible to predict and even specify such bars based on known perturbations for use with a nodal point relation such as that by *Bolla Pittaluga et al.* [2003]. For use of this relation to long-term calculations for bifurcations and avulsions in meandering systems, it was extended with the effect of spiral flow and the effect of the longitudinal bed slope. The transverse sediment flux predicted by the nodal point relation overestimates the flux calculated by the three-dimensional model even though $\alpha_W = 1$. As this was improved when the transverse flow discharge of the three-dimensional model was used, an improvement of the upstream asym-

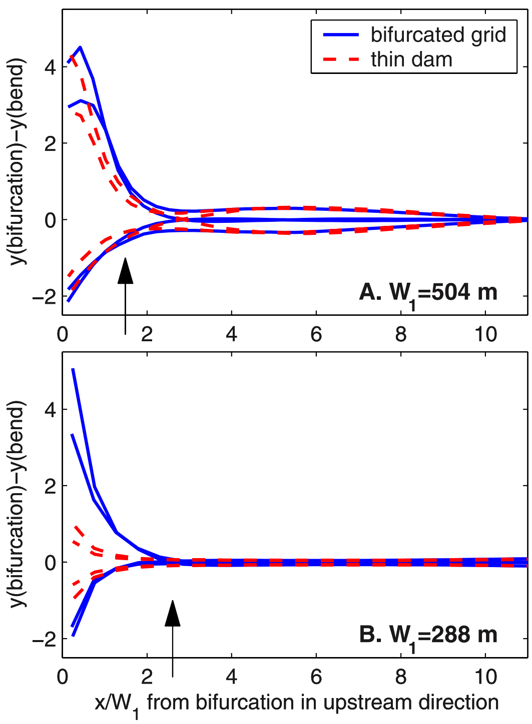

Figure 19. Upstream of the bifurcation on the morphology. Longitudinal bed level profiles of the left and right side of the upstream channels after 50 years are plotted. The bed levels are normalized by subtracting the bed levels in bended channels without bifurcations (series 7 in Table 1). The distance upstream of the bifurcation is normalized by dividing with the upstream channel width. The plotted runs are bifurcated grids (series 5 and 6) and thin dam grids (series 8) with both short and long upstream bends with widths of 504 m (a) and 288 m (b). The arrow indicates where the grid widening in the bifurcated grids starts (see section 3.5). All upstream bends have R/W_1 = 10 and equal downstream gradients.

metrical distribution over the cross-section of flow and bed topography seems a logical step. For instance, an upstream flow redistribution due to the alternating bar pattern could perhaps be introduced by predicting the bar wavelength and the distance from the perturbation. However, determining the location of the perturbation may be difficult in real rivers with groynes or natural banks and bars.

[108] Regarding the influence upstream, *Tubino and Bertoldi* [2005] identified an influence upstream of the bifurcation for the unstable bar regime, in addition to the obvious influence of the downstream boundary conditions. The question is whether the gradual transition of the bed level just upstream to downstream of the bifurcation is this influence upstream. Normalized longitudinal bed level profiles upstream of the bifurcation are plotted in Figure 19 for wide (unstable bar regime) and narrow (stable bar regime) channels and both types of grid representations. These results demonstrate that for both narrow and wide channels the influence upstream extends over a distance of 2 W_1. However, the narrow channel is not in the unstable bar regime with λ_s/λ_w = 0.5. This leads to the conclusion that there is a backwater influence upstream of the bifurcation but it is unrelated to the bar regime. The causes for the upstream influence of our model results are as follows. First, there is a numerical effect: the grid size affects the upstream length of influence (Figure 5). Second, the presence of a bluff and the widening of the bifurcated grid upstream of the bifurcation explains the larger influence upstream compared with the thin dam grids. Third, there is a deviation between the bends and bifurcations for the wider channels (Figure 19a) along the entire length of the upstream channel, but this is explained by the decreasing effective radius of the flow in the upstream bend while the inner-bend bifurcate closes off.

[109] Due to bar dynamics, the predictability of the direction of bifurcation evolution is inherently limited. This is particularly the case for bifurcations that are balanced by opposing factors, such as an upstream bend effect opposed by an increased slope in the bifurcate connected to the inner bend, and for bifurcations with wider and narrower upstream channels. For such cases the direction of evolution (which bifurcate closes off) is very sensitive to minor changes of topography at the bifurcation, downstream slopes, upstream bend radius, sediment transport predictor and so on. This is also due to the fact that effectively k = 1 for most of the time. Unstable bifurcations with a clearly favored branch, by a much larger slope or very sharp bend for instance, are relatively insensitive so that their direction of evolution can be predicted more easily. In practice, engineering structures at bifurcations may have effects on the direction of the evolution as well but these have not yet been studied well.

7.2. Applicability of Nodal Point Relations

[110] A number of hypotheses underlying nodal point concepts for one-dimensional models (section 2.5) were tested by the results of the three-dimensional model.

[111] For convenience in a theoretical analysis, *Wang et al.* [1995] assume a constant k independent of the stage of development of the closing and opening bifurcate, or both stable branches, and independent of flow conditions such as floods. The three-dimensional model shows that k changes during the evolution of the bifurcation from small values indicating unstable bifurcations to large values in the final stage indicating stable bifurcations with highly asymmetrical flow divisions. During floods k is highly variable. These results demonstrate that a model with a constant k cannot reflect the rich dynamics of three-dimensional-modeled and natural bifurcations. This has implications for many simulation models for braided rivers and for landscape and delta evolution. In many of these models the flow and sediment discharges are equally distributed over the three adjacent downstream cells entirely based on the local slope. If the flow and sediment discharge were divided with $k > 1$ and increasing k for increasing ratios of bifurcate discharges, then the models would perhaps give very different rivers, landscapes, deltas and alluvial architecture.

[112] Additionally, both the one-dimensional concepts and three-dimensional models do not account entirely satisfactorily for the suspended bed sediment load and not at all for wash load. First of all, in reality the suspended sediment vector is probably not deflected on a transverse slope. Second, it is deflected by spiral flow over the entire depth of the flow and modified according to the declining

sediment concentration away from the bed. However, since the spiral flow magnitude is very small compared with the main flow, the suspended sediment is divided at the bifurcation in about the same proportion as discharge (that is, $k = 1$). Ultimately, for bifurcates that are nearly closed off, only sediment far up in the water column flows and diffuses into the closing bifurcate. This is not so different from the modeled bed load behavior, but small gradients in the transport are enough to unbalance a bifurcation as there literally is no way back for the sediment once it enters a bifurcate. The balance of these effects is not known and transverse slope development including suspended sediment effects clearly needs more research. For now it must be assumed that these processes do not much affect the general behavior of the system.

[113] Nodal point relations developed so far remain more simplified representations than three-dimensional models because the character of the upstream channel is neglected in all nodal point concepts. *Bolla Pittaluga et al.* [2003] experimentally determined that the transverse slope just upstream of the bifurcation extends into the upstream branch over a length of <3 W_1 which remains constant over time. Based on this, they postulate that the transverse fluxes Q_y, Q_{sy} extend over the same distance. The new nodal point concept presented in section 2.4 is an extension of the *Bolla Pittaluga et al.* [2003] concept with a different transverse slope effect and a parameterization of spiral flow. The new relation assumes that sediment deflection by the spiral flow occurs over the same upstream length as the transverse slope. According to the three-dimensional model, the bed levels of the bifurcates do extend into the upstream branch for about 2 W_1 (Figure 6, lowest panel). However, on close inspection discrepancies were found between transverse flow and sediment fluxes in the three-dimensional model and according to the nodal point relations. The flow and sediment are redistributed over the width much further upstream due to the three-dimensional bar pattern that evolves in the upstream channel, in particular when the bars are underdamped. Perhaps nodal point relations could be incorporated in meander simulation models which account for the bar dynamics in bends.

[114] The three-dimensional modeling commonly resulted in highly asymmetrical bifurcations. These results contradict the general conclusions by *Bolla Pittaluga et al.* [2003] who found (more) symmetrical bifurcations for many conditions. Their slope effect counteracted sediment transport into the closing bifurcate so much that it kept both bifurcates open. One bifurcate was only closed in their model when the Shields number θ fell below the critical number and the initial conditions strongly favored one bifurcate. In the three-dimensional models the bifurcations are invariably unbalanced by even the most gentle upstream bend. The backwater effect in the three-dimensional model caused flow deceleration in the closing bifurcate once it had a shallower entrance (e.g., Figure 15), leading to the further closure (e.g., Figure 12). However, the development toward an asymmetrical discharge division also occurred for bifurcations with bifurcates much longer than the backwater adaptation length. Moreover, the slope effects in Delft three-dimensional and in the work of *Bolla Pittaluga et al.* [2003] are similar: both are a function of the transverse slope and of $\sqrt{\theta}$ where $\theta \approx 0.12$ in typical runs of $W = 504$ m. The *Engelund and Hansen* [1967] predictor used herein has no critical Shields number, but three-dimensional runs with transport predictors that had critical Shields numbers gave similar results so this did not affect the results. One major difference (apart from the one-dimensional versus three-dimensional model) is the much larger and more realistic width-depth ratios of the present models: 100 for the upstream branch with $W = 504$ m compared with 10–50 for the upstream branch in the work of *Bolla Pittaluga et al.* [2003, e.g., their Figure 8].

7.3. Implications for Bifurcation Stability and Avulsion Duration

[115] The three-dimensional model runs indicate that very few bifurcations close off entirely, but most bifurcations develop to a highly asymmetrical equilibrium configuration where most of the discharge is transferred to one of the bifurcates. The minor bifurcate then only discharges less than 5% of the flow and none of the upstream sediment transport. For finer grids, the asymmetry is even more pronounced but still the bifurcation stabilizes. When the bifurcates become longer than the backwater adaptation length (that is, when the distance between the downstream fixed water level condition and the bifurcation becomes longer), the bifurcation attains a more symmetrical discharge division, although an equilibrium was not reached in 200 years model time.

[116] The bar dynamics strongly affect bifurcation stability and avulsion duration, and may switch the main flow from one to the other bifurcate (Figure 11) in agreement with *Hirose et al.* [2003] and *Miori et al.* [2006a]. This has particularly implications for bifurcations and avulsions for which limited data are available (for instance, because they took place in the distant past). When the detailed initial bar topography and the location of a perturbation that initiates alternate bars are unknown or poorly constrained, it is impossible in practice to predict which bifurcate will become dominant for wider channels in the underdamped bar regime.

[117] The modeled duration of the avulsion time, here defined as increasing asymmetry phase (say, $1 < Q_i/Q_j < 10$, where $i, j = 2$ or 3 such that $Q_i \geq Q_j$) varies from 20 to much more than 200 years, which is an order of magnitude. This is partly determined by the width–depth ratio, the upstream bend radius, a gradient advantage for one bifurcate and the length of the bifurcates. Certain combinations of these parameters would further increase the avulsion time, such as a slightly larger slope of the inner-bend bifurcate with very long bifurcates and a sharp upstream bend. For otherwise constant parameters, an increase of bifurcate length leads to an equal increase of the avulsion time in agreement with *Bolla Pittaluga et al.* [2003], which can be understood as the time needed to fill up a bifurcate of varying length given a constant sediment feed. As such, the model explains how these variables may cause the large observed variation of avulsion duration in historical and geological data [*van de Ven*, 1976; *Smith et al.*, 1998; *Stouthamer and Berendsen*, 2001; *Makaske et al.*, 2002, Figure 1] in addition to other factors mentioned by these authors such as base level rise, wash load and tectonics.

[118] The effects of an upstream bend and of a downstream slope advantage of the bifurcate connected to the

inner bend counteract so that critical combinations exist where the bifurcates are balanced and quasistable for a long time. A slope advantage of about 20% is sufficient to cancel out an upstream bend with a radius of $R/W_1 = 10$. This finding is highly relevant because both the slope advantage and the bend radius are easily attained in nature. Near the critical combination of bend radius and slope, the model outcomes are very sensitive to small changes in the boundary conditions, sediment transport predictor, grid resolution and the way in which the bifurcation is represented. The precise critical combination therefore depends on various choices in the modeling, including numerical aspects that we did not test extensively. We do not claim to have calculated the precise critical combination; we have used a model with reasonable settings and choices to demonstrate that it exists for likely combinations of parameters. At the same time, this model uncertainty parallels the situation of natural bifurcations with a critical combination of bend radius and slope difference: such bifurcations will also be very sensitive to slight disturbances of morphology at the bifurcation or within a backwater adaptation length downstream thereof.

7.4. Assessing Effects of Bed Sediment Sorting and Channel–Floodplain Interactions

[119] Three major processes were neglected in the three-dimensional modeling that will affect the avulsion duration and bifurcation stability: bank erosion, levee and floodplain formation and bed sediment sorting.

[120] Rivers with poorly sorted sediment will develop vertical sorting in the bed, potentially armoring, and bend sorting. The sorting will affect sediment transport fluxes into the bifurcates as well as morphodynamic response [*Mosselman et al.*, 1999; *Kleinhans et al.*, 2007b]. The observed quasistability of the first and major bifurcation of the river Rhine may be explainable by a combination of armoring and bank protection. Over the past millennia, the Rhine gradually avulsed from a northern to a southern course. After many unsuccessful attempts to increase the flow discharge through the closing bifurcate, Dutch engineers dug a canal finished in 1707 to bypass the entrance of the nearly closed bifurcate. This canal had a larger slope than the other bifurcate and was favored with relatively more water and less sediment by its position in an outer bend. It enlarged so rapidly that the banks were protected hastily [*van de Ven*, 1976]. Accidently, the bed sediment consisted of sandy gravel deposited in earlier Holocene Rhine courses, which armored strongly [*Frings and Kleinhans*, 2008; *Kleinhans et al.*, 2007b]. As a result, the canal depth and width were constrained by heavy armoring and bank protection, which stabilized the flow and sediment division over the bifurcates. In conclusion, the bifurcation could not be stabilized by increasing the flow through the closing bifurcate, but could be stabilized (accidentally) by limiting the widening and deepening of the opening bifurcate.

[121] Bank erosion affects the flow capacity change of a bifurcate. During an avulsion, a new channel is created and widened through bank erosion. The eroded sediment must be removed, the rate of which depends on its caliber. Fines can easily be removed as wash load without greatly affecting the bed sediment transport capacity of the channel, but if the new channel is eroded in similar or coarser bed sediment this will take much more time. Meanders evolve by eroding banks as well, so that the bend radius at the bifurcation changes. In the river Rhine this happens at the same timescale as the bifurcation evolves: bends near the Dutch–German border migrate about one wavelength per 500 years. In cases of very sharp bends, e.g., against very cohesive banks, the flow may even separate from the bank [*Ferguson et al.*, 2003]. In such a case a vortex may develop over a significant part of the bifurcate width which promotes sedimentation in the bifurcate, as observed in several bifurcations during a field site visit by the first author in the Cumberland Marshes.

[122] Levee and floodplain formation also changes the capacity of the bifurcates to convey flow discharge, which further affects avulsion duration in nature. The closure of the old bifurcate commonly happens through shallowing by sedimentation near the channel entrance, as modeled in this paper, but also by narrowing. Yet levee and floodplain formation usually lag behind bank erosion. Hence the old channel downstream of the temporary bifurcation may narrow somewhat during the diversion of discharge, but is still nearly as wide as the channel upstream of the bifurcation in agreement with field data of meandering, braided and anastomosing rivers [e.g., *van de Ven*, 1976; *Mosselman et al.*, 1995; *Smith et al.*, 1998; *Makaske et al.*, 2002]. The models with a larger downstream width in the work of *Kleinhans et al.* [2006] show that the closure process is slower, which is due to the smaller sediment mobility in a shallower channel (although vegetation may enhance the process). Eventually residual channels may close off by filling with fines transported in as wash load (silt and clay) or vegetation and peat. To summarize, the width adaptation of the closing channel will increase avulsion duration. All issues discussed above need more research of combined fieldwork, experiments and modeling as argued in the work of *Kleinhans et al.* [2005].

7.5. Implications for Residual Channels and Anastomosing Rivers

[123] In agreement with the model results, there are many (geological) indications that bifurcates do not close off entirely for a long time but remain active as residual channels [*Smith et al.*, 1998; *Stouthamer and Berendsen*, 2001] that convey large discharges during floods [*van de Ven*, 1976; *Makaske et al.*, 2002] and may even be reactivated as major channels [*Stouthamer*, 2005; *Makaske et al.*, 2002]. The model results demonstrate that disproportionately large floods occur in the nearly closed bifurcates in agreement with historical records of the Nederrijn branch of the Rhine river [*van de Ven*, 1976] and of several historical tributaries of the Indus and Ganges [*Wilhelmy*, 1969]. A particular example is the former Sarasvati river (Hakra branch) which was fed by flood waters of the Sutlej river between 2600 and 700 years ago, and had completely dried out 400 years ago. The fact that bifurcates do not close off entirely for a long time implies a ‘‘leaky’’ river whereby the main active channel looses more and more discharge in the downstream direction through residual channels in addition to the usual crevasse and overbank flow. This interpretation is representative for avulsive settings such as the Cumberland Marshes, Saskatchewan River in Canada [*Smith et al.*,

1998] or deltaic settings such as the Holocene Rhine–Meuse delta in the Netherlands [*Stouthamer and Berendsen*, 2001].

[124] The results also apply to anastomosing and anabranching rivers [*Nanson and Knighton*, 1996] such as the Columbia River, Canada [*Makaske et al.*, 2002]. Although the appearance of anastomosing rivers is that of several active channels in terms of overbank deposition and flood conveyance, often only one channel at a time conveys most of the bed sediment [*Makaske et al.*, 2002; *Huang and Nanson*, 2007]. Thus only one channel bed is subject to significant morphological change as in the asymmetrical bifurcates modeled in this paper, although wash load and vegetation simultaneously modify the floodplains of all branches. Hence it may be more appropriate to define such rivers as single channel despite the presence of water in multiple channels that give such planforms their appearance.

7.6. Future Directions

[125] Since the work of *Wang et al.* [1995] the common wisdom is that bifurcation stability can be explained from a stability threshold for parameters of the nodal point relation. The present study suggests, however, that bifurcations always evolve to a very asymmetrical state, while persistently symmetrical bifurcations are related to quasiequilibria that result from a proper combination of upstream bend radius, channel width and downstream gradient, or to special conditions such as bank and bed protection in the bifurcate that would increase in size otherwise.

[126] Of course, reality is more complex than the model which is important for interpretation of field cases and for geological reconstruction, as well as for future work on bifurcations. Some, perhaps crucial, points are [also see *Kleinhans et al.*, 2005]:

[127] (1) The bar pattern of wider channels, and hence which bifurcate becomes dominant, is affected by perturbations of the channel planform. Such perturbations can be resistant patches of bank in an otherwise erosive stretch, large wood or human artifacts such as dams or groynes. E.g. 15th to 18th century engineers attempted to affect the discharge distribution at the Schenkenschans bifurcation of the river Rhine by several groynes upstream of the bifurcation [*van de Ven*, 1976].

[128] (2) The bed sediment may be sorted in the bend, leading to preferred feeding of coarse sediment to one bifurcate and fine sediment to the other [*Mosselman et al.*, 1999; *Kleinhans et al.*, 2007b; *Frings and Kleinhans*, 2008]. Moreover, bed surface armoring may stabilize bars.

[129] (3) The widening of new branches in nature depends on the bank erosion process, where the banks are erodible depending on the bank sediment composition, vegetation, etc. The widening also depends on the closure of the other bifurcate, which is affected by channel narrowing by levee deposition or bench formation from washload settling in the stagnant water at lower discharge, in addition to changing hydraulic roughness and downstream water levels, as well as by large wood deposited after floods, vegetation successions and, further downstream, peat development in the residual channel.

[130] (4) Meander migration changes the boundary conditions at the bifurcation. For wider channels, this also alters the bar pattern and associated flow pattern. Additionally, the bifurcation may migrate downstream with the eroding bends. This may lead to an increase of the angle between the dominant and the subordinate bifurcate, increasing the rate of changing asymmetry. Eventually the entrance angle of a bifurcate may become so large that the flow separates from the channel boundary.

[131] (5) Bifurcations near the sea or ocean are affected by tides propagating up the channels. Due to the energy gradient fluctuations combined with the nonlinear sediment transport, the tides enhance the sediment transport. Moreover, phase and amplitude differences between downstream water levels of the bifurcates enhance or counteract other differences between the bifurcates.

[132] (6) Downstream coast, estuary or delta development depends on the evolution (mostly cumulative sediment flux) of the bifurcates, and may in turn lengthen the bifurcate [*Swenson*, 2005].

8. Conclusions

[133] For a wide range of conditions and settings representative for meandering rivers, we conclude that bifurcations almost always attain a highly asymmetrical division of discharge and sediment. The division of sediment at the bifurcations is similar to the division of flow discharge during the phase of increasing asymmetry in all models, but eventually no sediment enters the subordinate bifurcate anymore so that it does not close off entirely. The choice which bifurcate becomes dominant, and the rate of change of bifurcation symmetry are determined by the following factors:

[134] (1) a gradient advantage of one bifurcate over the other increases the discharge through this channel;

[135] (2) a bend upstream of the bifurcation favors one bifurcate with relatively more flow discharge and the other bifurcate with relatively more sediment;

[136] (3) a gentle upstream bend can counteract downstream gradient advantages of 0–20% of the bifurcate connected to the inner bend, so that the flow and sediment division are equal and the bifurcation remains (quasi-) balanced;

[137] (4) the width–depth ratio of the upstream channel strongly determines the bar pattern and dynamics at the bifurcation and may lead to unstable bars and overdeepening, which may cause the flow to switch to the other bifurcate compared with cases with other widths;

[138] (5) sediment sorting, local bank irregularities, bank erosion and formation trends, possible scour holes or vortex bars just downstream of the bifurcation; and

[139] (6) boundary conditions and changes thereof at the same timescale as the bifurcation evolution.

[140] We identified realistic parameter settings for bends and slope advantages in which these competing factors are mutually balanced. For these cases the avulsion duration became an order of magnitude larger than for unbalanced cases. The model bifurcations, that were loosely based on the River Rhine in the Netherlands, became stably asymmetrical in periods of the order of a decade for unbalanced bifurcations to a few centuries for nearly balanced bifurcations.

[141] This offers an explanation why some bifurcations in the Holocene Rhine were destabilized within a few decades after their creation (fast avulsion) whereas other bifurcations were stable for many centuries (slow avulsion). It also

explains how bifurcates do not close off entirely but remain active as residual channels for a long time in agreement with geological data. Finally, it explains that anastomosing rivers have multiple channels that convey flow but have only one channel that conveys the bed sediment.

[142] Existing nodal point relations for one-dimensional models were evaluated against the three-dimensional model results, and one physics-based relation was improved by incorporating the effect of a meander bend just upstream of the bifurcation. However, the use of such relations is less successful particularly in wider and shallower channels with underdamped bars as these may switch the dominant channel of the bifurcation, so one-dimensional modeling with nodal point relations is most useful for relatively narrow and deep rivers.

Notation

A	spiral flow coefficient (–)
C	Chézy roughness coefficient ($\sqrt{\text{m}}$/s)
D	grain size (m)
g	gravitational acceleration (9.8 m/s^2)
h	water depth (m)
IP	interaction parameter (–)
k_s	Nikuradse roughness length (m)
L_D	damping length of bars (m)
L_p	wavelength of bars (m)
n	effective power on u to calculate sediment transport (–)
Q	flow discharge (m^3/s)
Q_s	width-integrated sediment transport (m^3/s)
q	specific flow discharge (m^2/s)
q_s	specific sediment transport rate (m^2/s)
R	meander bend radius (m)
r	factor in transverse slope effect (–)
S	channel slope (–)
u	flow velocity (s direction) (m/s)
v	flow velocity (n direction) (m/s)
W	channel width (m)
x	x coordinate (m)
y	y coordinate (m)
z	z coordinate (m)
α_W	relative length factor in nodal point relation (–)
β	direction relative to n-direction (rad)
ε	calibration coefficient for spiral flow intensity (O(1)–)
θ	nondimensional bed shear stress (Shields number –)
κ	Kármán's constant (0.4 –)
λ_{BW}	backwater adaptation length (m)
λ_s	adaptation length of a bed disturbance (m)
λ_w	adaptation length of the flow (m)
π	= 3.1415926535...
ρ	density of water (1000 kg/m^3)
ρ_s	density of sediment (2650 kg/m^3)
τ	bed shear stress (Pa)
1, 2, 3	branch numbers: 1 = upstream branch; 2, 3 = bifurcates
I	branch number index
50, 90	percentiles (for grain size)
K	power on discharge ratio in nodal point relation (–)
N	transverse flow direction
S	main flow direction (for τ)

[143] **Acknowledgments.** M. G. Kleinhans is supported by the Netherlands Earth and Life Sciences Foundation (ALW) with financial aid from the Netherlands Organization for Scientific Research (grant ALW-VENI-863.04.016). We sincerely thank E. Stouthamer, D. Smith, N. Smith, M. Tubino, R. Slingerland, G. Seminara, M. Yossef, and anonymous reviewers for stimulating discussion and comments. The authors contributed in the following proportions to conception and design, modeling, analysis and conclusions, and manuscript preparation: MK(40, 70, 50, 60%), HJ(20, 20, 10, 10%), EM(20, 0, 30, 20%), and CS(20, 10, 10, 10%).

References

Berendsen, H., and E. Stouthamer (2000), Late Weichselian and Holocene palaeogeography of the Rhine-Meuse delta, the Netherlands, *Palaeo*, *161*, 311–335.

Bertoldi, W., S. Miori, M. Salvaro, L. Zanoni, and M. Tubino (2006), Morphological description of river bifurcations in gravel-bed braided networks, in *River Flow 2006*, edited by R. Ferreira, E. Alves, J. Leal, and A. Cardoso, pp. 1311–1318, International Conference on Fluvial Hydraulics, Lisbon, Portugal, Taylor and Francis/Balkema, London, U. K.

Bolla Pittaluga, M., R. Repetto, and M. Tubino (2003), Channel bifurcation in braided rivers: Equilibrium configurations and stability, *Water Resour. Res.*, *39*(3), 1046, doi:10.1029/2001WR001112.

Bridge, J. (2003), *Rivers and Floodplains*, 491 pp., Blackwell, Oxford, UK.

Bulle, H. (1926), Untersuchungen über die Geschiebeableitung bei der Spaltung von Wasserläufen, *VDI Verlag*, Berlin.

Camporeale, C., P. Perona, A. Porporato, and L. Ridolfi (2005), On the long-term behavior of meandering rivers, *Water Resour. Res.*, *41*, W12403, doi:10.1029/2005WR004109.

Edmonds, D., and R. Slingerland (2007), Mechanics of river mouth bar formation: Implications for the morphodynamics of delta distributary networks, *J. Geophys. Res.*, *112*, F02034, doi:10.1029/2006JF000574.

Engelund, F., and E. Hansen (1967), *A Monograph on Sediment Transport in Alluvial Streams*, Teknisk Forlag, Kobenhavn, Denmark.

Federici, B., and C. Paola (2003), Dynamics of channel bifurcations in noncohesive sediments, *Water Resour. Res.*, *39*(6), 1162, doi:10.1029/2002WR001434.

Ferguson, R., D. Parsons, S. Lane, and R. Hardy (2003), Flow in meander bends with recirculation at the inner bank, *Water Resour. Res.*, *39*(11), 1322, doi:10.1029/2003WR001965, 1322–1333.

Frings, R., and M. Kleinhans (2008), Complex variations in sediment transport at three large river bifurcations during discharge waves in the river Rhine, *Sedimentology*, 1–27, doi:10.1111/j.1365-3091.2007.00940.x.

Hardy, R., S. Lane, R. Ferguson, and D. R. Parsons (2003), Assessing the credibility of a series of computational fluid dynamic simulations of open channel flow, *Hydrological Processes*, *17*, 1539–1560, doi:10.1002/hyp.1198.

Hirose, K., K. Hasegawa, and H. Meguro (2003), Experiments and analysis on mainstream alternation in a bifurcated channel in mountain rivers, in *River, Coastal and Estuarine Morphodynamics*, edited by A. Sánchez-Arcilla and A. Bateman, pp. 571–583, IAHR, Madrid.

Huang, H., and G. Nanson (2007), Why some alluvial rivers develop an anabranching pattern, *Water Resour. Res.*, *43*, W07441, doi:10.1029/2006WR005223.

Klaassen, G., E. Mosselman, and H. Brühl (1993), On the prediction of planform changes in braided sand-bed rivers, in *Advances in Hydro-Science and -Engineering*, edited by S. Wang, pp. 134–146, University of Mississippi, Washington.

Kleinhans, M., C. Buskes, and H. de Regt (2005), Terra Incognita: Explanation and reduction in earth science, *Int. Studies Philos. Sci.*, *19*(3), 289–317, doi:10.1080/02698590500462356.

Kleinhans, M., B. Jagers, E. Mosselman, and K. Sloff (2006), Effect of upstream meanders on bifurcation stability and sediment division in 1d, 2d and 3d models, in *River Flow 2006*, edited by R. Ferreira et al., pp. 1355–1362, International Conference on Fluvial Hydraulics, Lisbon, Portugal, Taylor and Francis/Balkema, London, U. K.

Kleinhans, M., H. Weerts, and K. Cohen (2007a), Evolution of a new tidal river bifurcation: numerical modelling of an avulsion after a catastrophic storm surge, in *River, Coastal and Estuarine Morphodynamics 2007*, edited by C. Dohmen-Janssen and S. Hulscher, pp. 815–822, Taylor and Francis/Balkema, London, U. K.

Kleinhans, M., A. Wilbers, and W. ten Brinke (2007b), Opposite hysteresis of sand and gravel transport up- and downstream of a bifurcation during a flood in the River Rhine, Netherlands, *Neth. J. Geosci.*, *86*(3), 273–285.

Kriele, H., Z. Wang, and M. de Vries (1998), Morphological interaction between the Yellow River and its estuary, in *Physics of Estuaries and Coastal Seas*, edited by J. Dronkers and M. Scheffers, pp. 287–295, 8th International Biennial Conference on Physics of Estuaries and Coastal Seas, The Hague, Netherlands, 1996, Taylor and Francis/Balkema, London, U. K.

Lesser, G. R., J. A. Roelvink, J. A. T. M. van Kester, and G. Stelling (2004), Development and validation of a three-dimensional morphological model, *J. Coastal Eng.*, *51*, 883–915.

Makaske, B., D. Smith, and H. Berendsen (2002), Avulsions, channel evolution and floodplain sedimentation rates of the anastomosing upper Columbia River, British Columbia, Canada, *Sedimentology*, *49*, 1049–1071.

Meyer-Peter, E., and R. Mueller (1948), Formulas for bed-load transport, in *Proceedings 2nd Meeting*, pp. 39–64, Int. Ass. for Hydraulic Structures Res., Stockholm, Sweden.

Miori, S., R. Repetto, and M. Tubino (2006a), Unsteadiness effects on the morphological behaviour of gravel-bed river bifurcation, in *River Flow 2006*, edited by R. Ferreira et al., pp. 1283–1291, International Conference on Fluvial Hydraulics, Lisbon, Portugal, Taylor and Francis/Balkema, London, U. K.

Miori, S., R. Repetto, and M. Tubino (2006b), A one-dimensional model of bifurcations in gravel-bed channels with erodible banks, *Water Resour. Res.*, *42*, W11413, doi:10.1029/2006WR004863.

Mosselman, E., M. Huisink, E. Koomen, and A. Seymonsbergen (1995), Morphological changes in a large braided sand-bed river, in *River Geomorphology*, edited by E. Hickin, pp. 235–247, Wiley.

Mosselman, E., J. Sieben, K. Sloff, and A. Wolters (1999), Effect of spatial grain size variations on two-dimensional river bed morphology, pp. 499–507, IAHR symposium on River, Coastal and Estuarine Morphodynamics.

Mosselman, E., M. Tubino, and G. Zolezzi (2006), The overdeepening theory in river morphodynamics: Two decades of shifting interpretations, in *River Flow 2006*, edited by R. Ferreira et al., pp. 1175–1181, International Conference on Fluvial Hydraulics, Lisbon, Portugal, Taylor and Francis/Balkema, London, U. K.

Nanson, G., and A. Knighton (1996), Anabranching rivers: their cause, character and classification, *Earth Surf. Processes Landforms*, *21*, 217–239.

Parker, G., O. Sequeiros, and River Morphodynamics Class of Spring 2006 (2006), Large scale river morphodynamics: Application to the Mississippi Delta, in *River Flow 2006*, edited by R. Ferreira et al., pp. 3–11, International Conference on Fluvial Hydraulics, Lisbon, Portugal, Taylor and Francis/Balkema, London, U. K.

Schoor, M., H. Wolfert, G. Maas, H. Middelkoop, and J. Lambeek (1999), Potential for floodplain rehabilitation based on historical maps and present-day processes along the River Rhine, Netherlands, in *Floodplains: Interdisciplinary approaches, Special Publication*, vol. 163, edited by S. Marriott and J. Alexander, pp. 123–137, Geological Society, London, U. K.

Slingerland, R., and N. Smith (1998), Necessary conditions for a meandering-river avulsion, *Geology*, *26*(5), 435–438.

Smith, N., R. Slingerland, M. Pérez-Arlucea, and G. Morozova (1998), The 1870's avulsion of the Saskatchewan River, *Can. J. Earth Sci.*, *35*(4), 453–466.

Stelling, G., and J. Leendertse (1991), Approximation of convective processes by cyclic ACI methods, in *Proceedings 2nd ASCE Conference on Estuarine and Coastal Modelling*, ASCE, Tampa.

Stouthamer, E. (2005), *Reoccupation of Channel Belts and Its Influence on Alluvial Architecture in the Holocene Rhine-Meuse Delta, The Netherlands*, vol. 83, pp. 319–339, Society for Sedimentary Geology.

Stouthamer, E., and H. J. A. Berendsen (2000), Factors Controlling the Holocene Avulsion History of the Rhine-Meuse Delta (The Netherlands), *J. Sediment. Res.*, *70*(5), 1051–1064, doi:10.1306/033000701051.

Stouthamer, E., and H. J. A. Berendsen (2001), Avulsion frequency, avulsion duration, and interavulsion period of Holocene channel belts in the Rhine-Meuse delta, the Netherlands, *J. Sediment. Res.*, *71*(4), 589–598, doi:10.1306/112100710589.

Struiksma, N., K. Olesen, C. Flokstra, and H. D. Vriend (1985), Bed deformation in curved alluvial channels, *J. Hydraul. Res.*, *23*(1), 57–79.

Swenson, J. (2005), Relative importance of fluvial input and wave energy in controlling the timescale for distributary-channel avulsion, *Geophys. Res. Lett.*, *32*, L23404, doi:10.1029/2005GL024758.

Talmon, A. M., N. Struiksma, and M. C. L. M. van Mierlo (1995), Laboratory measurements of the direction of sediment transport on transverse alluvial-bed slopes, *J. Hydraul. Res.*, *33*(4), 495–517.

Tubino, M., and W. Bertoldi (2005), Bifurcations in gravel-bed streams, *Gravel Bed Rivers*, *6*, 1–28.

van de Ven, G. (1976), *Aan de wieg van Rijkswaterstaat-wordingsgeschiedenis van het Pannerdens Kanaal (in Dutch)*, 438 pp., De Walburg Pers, Zutphen, Netherlands.

Van den Berg, J. (1995), Prediction of alluvial channel pattern of perennial rivers, *Geomorphology*, *12*, 259–279.

Van Rijn, L. (1984a), Sediment transport: Part I. Bed load transport, *J. Hydraul. Eng.*, *110*(10), 1431–1456.

Van Rijn, L. (1984b), Sediment transport: Part II. Suspended load transport, *J. Hydraul. Eng.*, *110*(11), 1613–1641.

Wang, Z., R. Fokkink, M. D. Vries, and A. Langerak (1995), Stability of river bifurcations in 1D morphodynamic models, *J. Hydraul. Res.*, *33*(6), 739–750.

Wilhelmy, H. (1969), Das Urstromtal am Ostrand der Indusebene und das Sarasvati-Problem (in German), *Z. Geomorphol.*, *8*, 76–93.

H. R. A. Jagers, E. Mosselman, and C. J. Sloff, Deltares (formerly WL Delft Hydraulics), P.O. Box 177, 2600 MH Delft, Netherlands. (bert.jagers@deltares.nl; erik.mosselman@deltares.nl; kees.sloff@deltares.nl)

M. G. Kleinhans, Faculty of Geosciences, Department of Physical Geography, Utrecht University, P.O. Box 80115, 3508 TC Utrecht, Netherlands. (m.kleinhans@geo.uu.nl)